# AN INTEGRAL FIELD INFRARED SPECTROMETER FOR THE NEXT GENERATION SPACE TELESCOPE

**J. R. Graham (UC, Berkeley), M. C. Abrams (ITT)**
**C. L. Bennett (LLNL), J. Carr (NRL),**
**K. Cook (LLNL), A. Dey (NOAO),**
**R. J. Hertel, N. H. Macoy (ITT)**
**S. Morris (Herzberg Institute of Astrophysics)**
**J. Najita (NOAO), A. Villemaire (ABB BOMEM Inc.)**
**E. H. Wishnow, R. Wurtz (LLNL)**

September 1, 1999

# Contents

# 1 Executive Summary

The scientific mission of the Next Generation Space Telescope (NGST) is grand and visionary, defined by broad and ambitious goals: to measure the fundamental cosmological parameters of the universe; to observe the first galaxies and map out their history to the present epoch; to trace the production of the chemical elements in stars; and to understand the formation and evolution of stars and planets (Stockman 1997). While its singular abilities will place NGST at the threshold of tremendous discovery, its uniqueness requires that it be sufficiently equipped to follow up its own discoveries, to put the discoveries in context, and to define and achieve its science goals largely independently of other observatories. For example, NGST alone will be capable of surveying the formation and evolution of galaxies. This situation contrasts with that of the Hubble Space Telescope where the nature of galaxies in the Hubble Deep Field was revealed by spectroscopy with the 10-m Keck telescopes. Ground-based NGST followup would require apertures >30 m; such telescopes are being discussed but their technological readiness is uncertain, and none are yet planned.

To achieve its science goals NGST must be able to image and measure spectra of large samples of objects. Imaging establishes the brightness, morphology, and spatial correlation of sources, and spectroscopy is used to determine masses, ages, chemical compositions, redshifts and kinematics. Large samples are needed to solve the complex astronomical problems that NGST has targeted. For example, they are necessary to map with some degree of statistical precision the complex evolutionary history of the diverse population of galaxies, i.e., to study galaxies over a wide range in redshift, morphology, environment, mass, age, chemical enrichment, and star formation rate. The detailed study of these inter-dependencies, e.g., of galactic star formation history on environment, is critical in order not only to chart the diversity of galaxy evolutionary histories, but more significantly, to deduce the input physics that gave rise to the observed phenomena.

In this report, we demonstrate that these goals are well matched to the capabilities of IFIRS (Integral Field Infra-Red Spectrometer), an imaging Fourier transform spectrometer (IFTS). An IFTS combines the functions of a camera and a spectrometer, acquiring simultaneous deep imaging and spectroscopy for every object in the field of view. This unconventional solution to the need for imaging and spectroscopy of large samples is driven by the unique region of parameter space that NGST will occupy: the IFTS makes optimal use of the high number density of objects accessible to NGST at the faint flux levels that it will reach. Since deep number counts are in excess of $10^6$ objects per square degree at a flux level of 35 nJy, the IFTS instrument, IFIRS can obtain 1-5 $\mu$m ($R = 100$, $10\sigma$) spectra for a complete sample of $10^4$ objects in $10^5$s. An order of magnitude fewer galaxy spectra would be acquired in the same time with a conventional grating-based multi-object spectrograph (assuming 100 slits), which would require multiple grating settings and slit mask setups to produce the equivalent data set. In the latter case, additional time would be needed to carry out a multicolor imaging survey from which objects would be selected for spectroscopic study. The advantage of the IFTS over a slit-based multi-object spectrometer (MOS) system for spectroscopic surveys increases rapidly due to the growing object number density with depth.

The IFTS has, in addition, numerous advantages compared to traditional approaches:

• **Efficient Surveys** Operationally, an IFTS is well suited to the large photometric ($R \simeq 10$) and low resolution spectroscopic ($R \simeq 100$) surveys required to accomplish the NGST science goals. Large spectroscopic surveys traditionally have significant overheads since images are first obtained and objects are then selected for spectroscopic study. An IFTS breaks this paradigm by acquiring imaging spectroscopy for every object in the field of view; the need for target selection is thereby eliminated. Additional operations such as slit mask alignment are also eliminated, and the cost and complexity of planning and scheduling spectroscopic observations are much reduced. By offering a dispersed FTS mode, IFIRS extends the spectroscopic resolution to $R \simeq 5000$ with a sensitivity that is identical to a classical dispersive system. IFIRS can carry out the *entire* NGST DRM in significantly less (69%) time than that estimated for the Yardstick ISIM (§2.4).

• **A Serendipity Machine** By eliminating target selection, the IFTS naturally produces spectroscopically complete surveys and avoids the need for the often time-consuming task of quantifying selection biases. At the same time, it lends to the spectroscopic capability the same potential for serendipity that is normally accorded only to imaging. Thus, it is a powerful tool for discovery.

• **Simultaneous Deep Imaging** By combining the capabilities of camera and spectrometer, IFIRS simultaneously acquires deep panchromatic imaging along with multi-object spectroscopy. For example, in the $10^5$s example given above, IFIRS simultaneously acquires a deep $1-5$ $\mu$m image (0.2 nJy, $SNR$=10). In a traditional approach, an additional $10^5$ s exposure with a separate imager would be required.

• **Broad Wavelength Coverage** The visible through mid-IR coverage of NGST is critical to the success of the mission (e.g., the study galaxy properties over a large redshift range (§2.1); but it also presents challenges to traditional approaches of implementing spectroscopy over a large wavelength range. An IFTS can deliver spectroscopy over the entire wavelength range, simultaneously and for all objects in the field of view. Typically, three times as many gratings as beam-splitters are needed to cover the same wavelength range, resulting in increased mass, complexity, and cost.

• **Precise Spectrophotometry** Because slits are not used, there are no slit losses and precise spectrophotometry can be obtained over an extremely large wavelength range. This capability is critical to the success of NGST programs such as the study of SNe as standard candles (§2.2.1).

• **Simultaneous Science** Due to the spatial multiplexing capability of the IFTS, projects normally conceived as separate programs can be carried out simultaneously, thereby increasing efficiency. For example, while carrying out galaxy evolution surveys, IFIRS can discover, classify, and measure the redshifts and photometric properties of $\simeq 24$ supernovae per field of view with $\langle z \rangle \simeq 1.5$ in each deep $10^5$ exposure (see §2.2.1).

• **Spectral Deconvolution of Crowded Fields** Since complete imaging and spectroscopy are acquired, an IFTS also offers the capability of separating the spectra of objects in crowded fields through deconvolution in the image plane. This capability is critical at the low flux density levels that NGST will reach where galaxy overlaps are common (e.g., Fig. 4).

• **Flexibility for the Future** Given the rapid rate of change in astronomy, NGST at launch may face new scientific challenges beyond those contemplated today. By virtue of its flexible wavelength coverage and spectral resolution, an IFTS is highly adaptable to the

requirements of future programs.

As we demonstrate in the next section, many of the programs that form the scientific basis for NGST would benefit greatly from the capabilities of IFIRS and the specific advantages outlined above.

### 1.1 Overview of the IFIRS Concept

IFIRS is a Michelson interferometer configured as an IFTS (See Fig. 1) (Bennett 1993; Graham et al. 1998; Graham et al. 2000).[1] A moving mirror introduces an optical path difference (OPD) between the two beams created by the beam-splitter; the resulting interferogram from the combined beams is recorded for every pixel in the field of view, and hence a spectrum is obtained for every object. Since the bandpass of the instrument is defined only by the detectors and the efficiency of the beam-splitter, broad wavelength coverage is an intrinsic feature of the IFTS. An IFTS has continuously variable spectral resolution up to a maximum defined by the maximum OPD, which in the IFIRS design is 1 cm (i.e., $R_{max} = 10,000$ at 1 $\mu$m). IFIRS is a four-port interferometer, a choice which yields several advantages. (1) Virtually all the light collected by the telescope is directed toward the focal plane for detection. (2) The final interferogram, constructed from the difference of the two output ports, is immune to common mode noise.

When the interferograms from the two output ports are summed, the total flux image is recovered, producing the simultaneous deep panchromatic image that is a unique capability of an IFTS. In comparison with a simple camera, in which the panchromatic image would be formed by summing individual filter images, the IFTS panchromatic image has a speed advantage factor equal to the number of filters used.[2] In its hybrid, or dispersed FTS mode, designed for use with slit masks at high spectral resolution ($R \simeq 600 - 10,000$), IFIRS delivers a sensitivity for each object equivalent to that of a conventional dispersive spectrograph, with the spatial multiplex advantage of a multi-object spectrometer.

## 2 IFIRS & NGST Science

Due to its flexibility, IFIRS can efficiently accomplish the entire NGST science program. Since NGST must obtain images and spectra of large samples of objects in order to achieve its science goals, IFIRS' ability to deliver diffraction-limited full-field imaging spectroscopy is a critical advantage. Fig. 2 compares the noise equivalent flux density (NEFD) per pixel as a function of spectral resolution for NGST backgrounds at 2 $\mu$m for a tunable filter camera (e.g., a Fabry-Perot or a filter wheel camera), a dispersive spectrometer, and an IFTS (Bennett 2000). At the lowest spectral resolution, all of the instruments converge to a common performance. The dispersive spectrometer has the best performance for spectroscopy, although only for the small number of objects that may be contained within the slit. Although multi-slits and IFUs can target more objects than a single long slit, the number of objects that can be studied is limited to a small fraction of the total number in the field of view in typical deep NGST exposures. For imaging in a single narrow band, the single setting tunable filter provides an

[1] See also http://astron.berkeley.edu/~jrg/ngst

[2] http://astron.berkeley.edu/~jrg/ngst/trades/spectrometer_trades.html

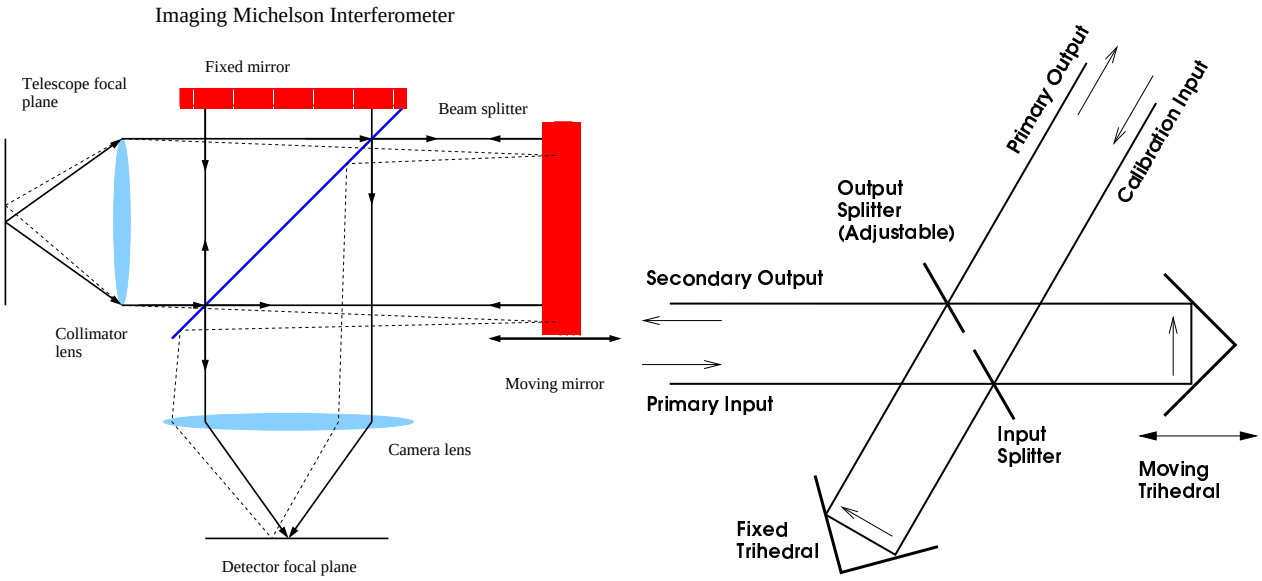


Figure 1: **Left:** In an IFTS, the telescope focal plane is imaged onto a detector array for high angular resolution imaging and spectroscopy. **Right:** IFIRS adopts a four-port design in which all photons are directed to a focal plane array for detection. Cube-corners displace the input and output beams.

Table 1: **Observational Capabilities of IFIRS**

| | Near-IR Channel | Mid-IR Channel |
|---|---|---|
| Bandpass/Detector | 0.6-5.6 $\mu$m/InSb | 3-28 $\mu$m/Si:As |
| Maximum Spectral Resolution,$R^a$ | 15,000 | 3000 |
| FOV/Array Format | $5.'28$/8k×8k | $2.'64$/2k×2k |
| Pixel size/Nyquist sampled $\lambda$ | $0.''0386$/3 $\mu$m | $0.''0772$/6 $\mu$m |
| Wavefront error/Strehl$^b$ | 150 nm rms/0.8 | 150 nm rms/0.99 |
| Throughput (excluding detector) | 86% | 87% |
| FTS Sensitivity$^{a,b}$, $R^{b,c}=1/5/100$ | 0.2/1/35 nJy | 13/65/1300 nJy |
| Dispersed FTS Sensitivity$^{b,c}$, $R^c=600$ | 66 nJy | 1080 nJy |

$^a$Spectral resolution, $R$, is the number of independent spectral channels in the band-pass.
$^b$The near- and mid-IR Strehl ratios and sensitivities are quoted at 2 & 10 $\mu$m respectively.
$^c SNR = 10$, $t = 10^5$ s for a total system efficiency of 50%, including detector QE, and an OTA with an 8-m primary, 71% filling factor, and 5 gold surfaces. All near-IR or mid-IR spectral channels are obtained simultaneously.

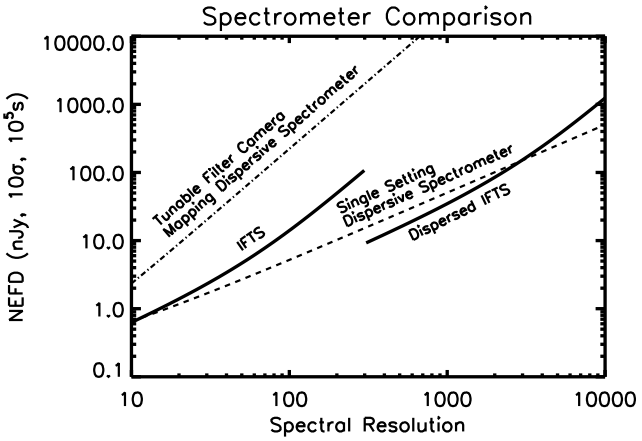


Figure 2: The NEFD per pixel for a variety of imaging spectrometer approaches on NGST from Bennett (2000). All observations extend over the $K$-band, and assume an observation time of $10^5$ s. The IFTS obtains spectra for every pixel in the field at the stated resolution. The IFTS curve for $R > 300$ is for the dispersed IFTS option, and assumes the addition of a prism in collimated space and a slit at an image plane. The mapping dispersive spectrometer is scanned over a number field of view settings, assumed to be equal to the number of spectral channels acquired by the tunable filter camera, and thus they have equal NEFD. The single setting dispersive spectrometer acquires spectra for a single pointing. The same NEFD level is achieved by a tunable filter camera if all the integration time is devoted to observing a single wavelength. The detector performance parameters are: 15 $e^-$ rms read noise per read, 0.1 $e^-$ $s^{-1}$ dark current. The time per readout is assumed to be 10 s.

NEFD performance equivalent to that of the dispersive spectrometer, but for every pixel in the field of view. For the purpose of obtaining complete spectra for every pixel in the field of view, the IFTS substantially outperforms both the tunable filter and the dispersive spectrometer used in mapping mode.

For $R \gtrsim 10^3$, the relatively bright sources required for good SNR imply that many fields of interest to NGST will only have about $10^3$ targets per field of view. In this situation, it is not necessary to obtain spectra for every pixel in the field of view. A hybrid approach (e.g., Beer 1992), which takes advantage of the best features of all of the 3-d imaging approaches, is the combination of an objective prism with an IFTS. A relatively modest dispersion across one dimension of the image plane serves to reduce the spectral bandpass acceptance that is involved in the noise term for the IFTS. With a slit at an image plane, the panchromatic output of the IFTS would yield the same results as an ordinary prism spectrometer, while the Fourier transformed interferograms would enable much higher spectral resolution at much reduced NEFD. The $R > 300$ segment of the FTS curve in Fig. 2 is for this hybrid configuration, and corresponds to the addition of an $R \simeq 600$ dispersing prism and a focal plane mask.

The curves would vary slightly depending on the choices for the detector performance parameters and system efficiency values. Using the NGST detector performance goals for read noise and dark current, instead of the current performance values, would improve the sensitivity of the tunable filter, the dispersive spectrometer, and the dispersed IFTS, but produces little change in the IFTS.

In conclusion, the ability of a single instrument, composed of a filter wheel, programmable

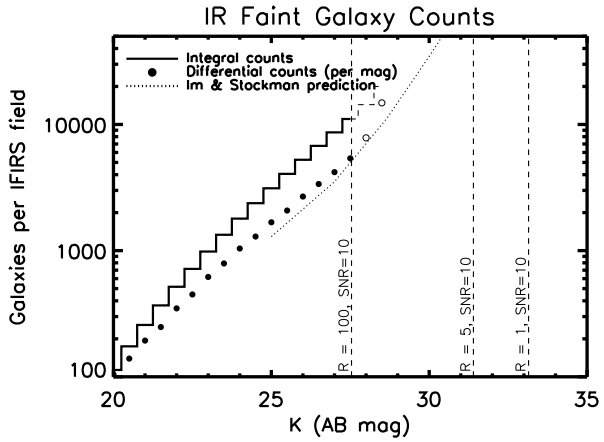


Figure 3: Merged faint galaxy counts from Yan et al. (1998) for $H < 25.9$ AB, Bershady et al (1998) for $K < 24.9$ AB, Thompson et al (1999) for $H < 28.8$ AB, and HDF-S. The data have been corrected for incompletness according to Thompson et al. Beyond $K = 27.5$ AB the data are plotted as a dashed line or open symbols indicating where uncertainties are significant ($\gtrsim \times 2$) due to small field observed by NICMOS, photometric errors, and statistical errors. The IFIRS $SNR = 10$ thresholds for deep exposures ($10^5$ s) at $R = 1$, 5, & 100 at $K$ are indicated by the dashed lines.

focal plane mask, dispersive prism, and Michelson interferometer, to deliver the performance of a wide field diffraction limited camera; a moderate resolution, full field imaging spectrometer; and a high resolution, multi-object spectrometer, makes IFIRS a compelling choice for NGST. In the rest of this section, we show that IFIRS is well-matched to the NGST science goals. We first consider the NGST science themes, discussing their scientific requirements in the context of IFIRS capabilities. We then summarize the results of our analysis of the NGST Design Reference Mission (DRM): IFIRS can carry out the *entire* NGST DRM in significantly less time than estimated for the Yardstick ISIM (§2.4).

## 2.1 The Origin and Evolution of Galaxies

The cornerstone of NGST's scientific mission is its goal to understand the formation and evolution of the galaxy population. With its low background and high sensitivity, NGST is uniquely positioned to investigate the formation of the first galaxy fragments, their growth (by merging) into galaxies, and the subsequent chemical and dynamical evolution into the Hubble sequence that we observe at the present epoch. These science goals are addressed by five conventional imaging and spectroscopic surveys (proposed by Lilly et al.) in the DRM on the Origin and Evolution of Galaxies. The surveys target relatively large samples of galaxies: imaging is required to determine morphology and select spectroscopic samples, low resolution $R = 100$ spectroscopy of large samples targets global galaxian properties (e.g., redshifts, star formation rate, mean stellar age), and higher resolution $R = 1000$ spectroscopy of smaller samples to determine metallicities, stellar content, dynamical masses, and dust content.

IFIRS is optimized to carry out all aspects of these studies. The steeply rising galaxy number counts (Fig. 3) suggest that the NGST focal plane may be crowded with $\sim 10^5$ faint galaxies per $5.'28 \times 5.'28$ FOV, i.e., one object per square arcsecond! The efficient study of objects at high surface densities necessitates a highly multiplexed approach, such as that

afforded by IFIRS. Imaging and low-resolution spectroscopy of the fainter objects can be carried out simultaneously in the regular IFTS mode; the higher resolution measurements would be carried out in the dispersed FTS mode. IFIRS' ability to simultaneously carry out the imaging and low spectral resolution studies not only increases the overall efficiency of the observatory, but also greatly enhances the discovery potential within the FOV and the ability to combine different science programs in a single observation.

To demonstrate the ability of IFIRS to detect and study faint objects we have simulated data as follows. An astronomical scene is represented as a noise-free distribution of objects and associated spectra. This input data cube is convolved with the telescope point spread function (PSF). The spectra are then multiplied by the wavelength dependent throughput. From this spectral data cube the interferogram cube is calculated by a Fourier transform, and noise is added at each OPD step. The noise sources treated are photon shot noise (from the zodiacal light, the target object, and thermal emission from the telescope), shot noise due to detector dark current, and detector read-noise. The noise-added interferogram cube is then Fourier transformed back into a spectral data cube.

Figure 4 shows simulated data resulting from a $10^5$s, $R = 100$, $1 - 5\mu$m IFIRS observation of a small section ($4\farcs9 \times 4\farcs9$; corresponding to 0.02% of the IFIRS field of view) of the Im & Stockman (1998) NGST deep field. This subfield contains a $K = 26.0$ AB mag $z = 4.67$ spiral and 60 $z > 5$ star-forming galaxies brighter than $K \approx 33.5$ AB mag. Crowding is significant: at least 6 of the $z > 5$ galaxies lie behind the spiral, and several others are obscured by other foreground galaxies. We have added a SN Ia to the spiral and a $z = 12$ proto-cluster. The proto-cluster has $F_\nu = 2$ nJy, and has been forming stars at a rate of 2.5 $M_\odot$ yr$^{-1}$ for $10^7$ yr.

The extracted IFIRS spectrum of the $z = 12$ proto-cluster clearly shows the Ly$\alpha$ line, the continuum longward of the line, and the continuum break across the line (due to intervening hydrogen). The detection of emission lines will allow IFIRS to measure redshifts and star formation rates. Given the large number of objects that will be simultaneously observed and the deep imaging and spectroscopy that will be available for each object, it will be possible to map out the co-evolution of the star formation and morphological evolutionary history of galaxies. All objects brighter than 0.15 nJy are detected in the deep $1 - 5\mu$m panchromatic image that is obtained simultaneously. The statistics of the deep image illustrate the approach to the crowding limit and the diagnostic power of panchromatic imaging: approximately 33% of the pixels in the panchromatic image are "filled", i.e., have values $> 5\sigma$ above sky. The simulated data illustrate the speed with which IFIRS will be able to carry out the imaging and spectroscopic surveys, the high quality data that IFIRS will produce, and the need for IFIRS' full field spectroscopic ability to spectrally and spatially separate background objects from foreground ones.

In the following subsections, we highlight some of the science gains of IFIRS over traditional instrumentation.

### 2.1.1 Growth of Structure

The redshift evolution of galaxy clustering is a fundamental test of all structure formation theories. The amount and form of clustering in a galaxy population can be estimated from a redshift survey (e.g., Fig. 5) using a variety of sophisticated statistical measures, the simplest of which is the two-point correlation function $\xi$ (or its Fourier analog, the spatial power spectrum). Formal error estimates for $\xi$ scale as the square root of the number of galaxies in

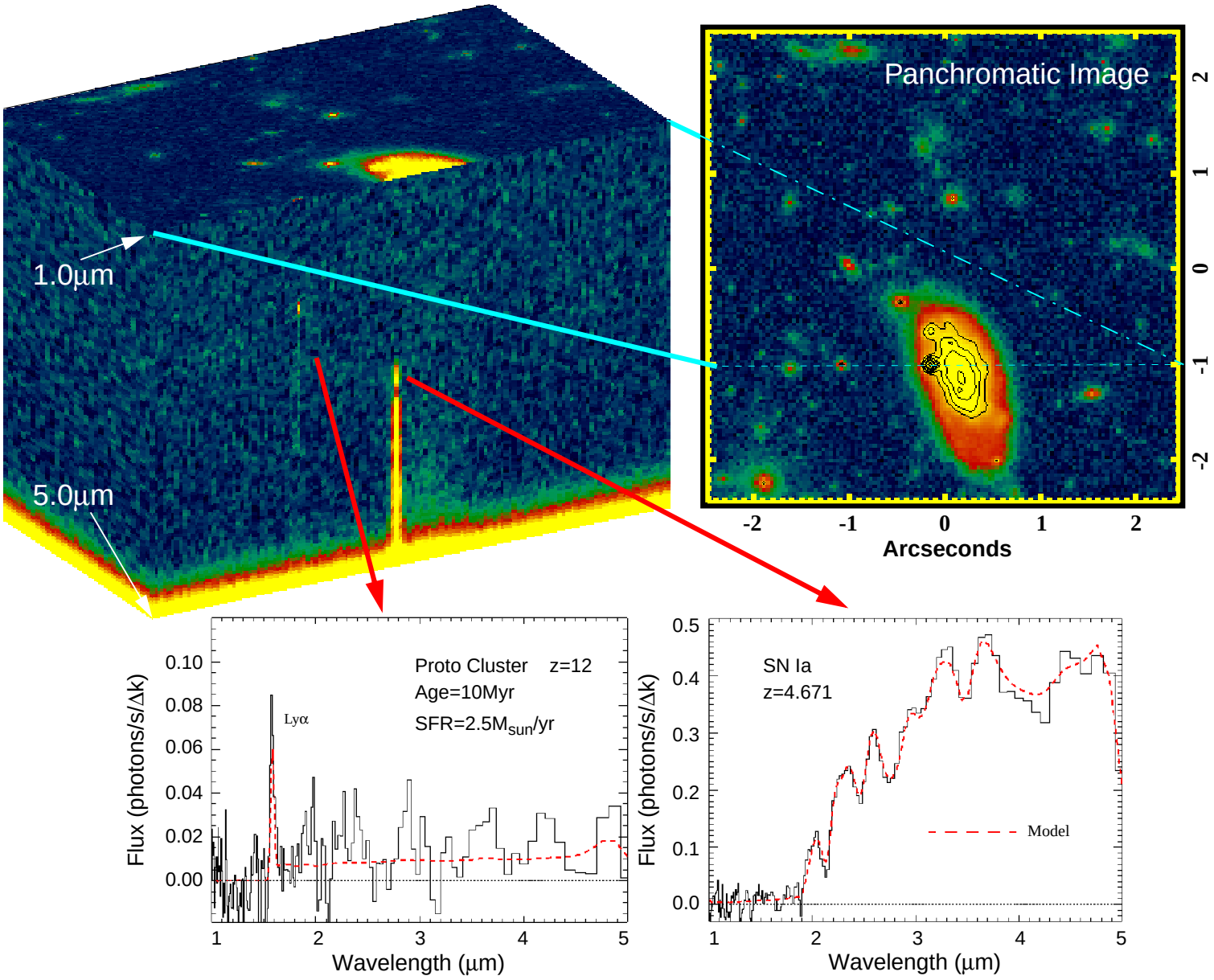


Figure 4: A simulation of a $10^5$ s $R = 100$ $1 - 5$ $\mu$m NGST/IFIRS observation. The resulting data cube, associated panchromatic image, and spectral extractons are displayed. Only $4\farcs9 \times 4\farcs9$ (i.e., 0.02% of the IFIRS FOV) is shown. The input data is a portion of the NGST Deep Field simulation by Im & Stockman (1998). The 3-d IFIRS data cube (top left) has been sliced open to reveal the spectra of a $z$=12 star forming proto-cluster and a $z$=4.67 SN Ia (the redshift corresponds to that of the spiral galaxy). In the panchromatic image from this observation (top right), the horizontal dashed line shows the position at which the cube is sliced open. The extracted spectra of the proto-cluster and the SN Ia are shown at bottom left and bottom right along with the input model spectra (red dashed line). The NEFD at 3 $\mu$m is about 3 nJy, 1 $\sigma$ so the $SNR$ for the cluster is about 0.6 and 17 for the SN.

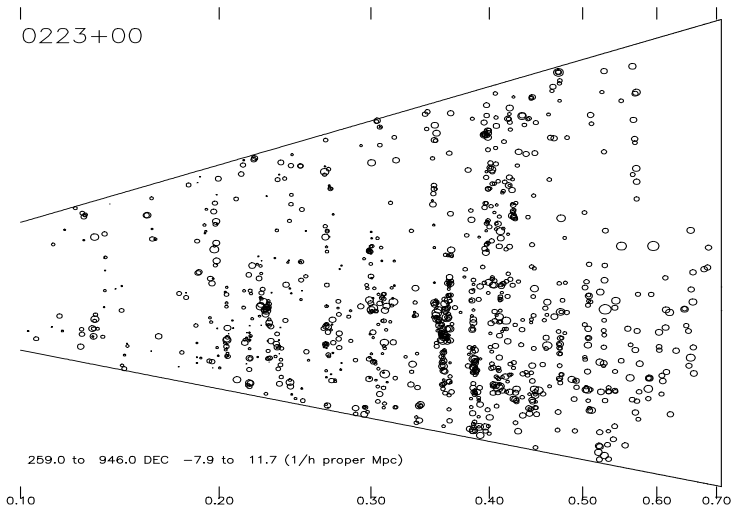


Figure 5: A pie section showing about 1500 galaxies in one of the 2° fields of the CNOC2 survey (Carlberg et al. 1999). Galaxy redshifts, from 0.1 to 0.7, are plotted along the $x$-axis. The opening angle of the slice has been expanded to reveal the individual points. One can see structure emerging, and statistically significant clustering studies are feasible. IFIRS will produce redshifts for thousands of galaxies per field over a vastly greater redshift range, rendering NGST extremely effective for studying the evolution of structure. A conventional MOS survey will measure only a few hundred redshifts per pointing, and thus is much less suited for these studies.

each redshift bin, and so very large samples are needed. Samples of a few hundred galaxies resulting from conventional MOS surveys in a particular field will be entirely inadequate to address this problem. The need for large samples is made more extreme by the vastly extended redshift range probed by NGST and by the clear desire to subdivide any galaxy sample still further to look for clustering as a function of galaxy properties such as luminosity, color, star formation rate, or morphology (cf. Kauffmann et al. 1999). For such studies, sample sizes of $\sim 10^5$ objects, much larger than estimated in the Galaxy DRM proposals, are needed and feasible (!) with the spatial multiplexing capability of IFIRS.

Since IFIRS deep field observations produce large numbers of redshifts in a *single* field, isolating correlated structures (clusters, filaments, sheets) in redshift space is automatic. Hence, IFIRS will enable the investigation of various relations (e.g., morphology vs. density, star formation rate vs. density) in coherent structures and trace the evolution of these relations as a function of redshift. IFIRS surveys in the regions of rich galaxy clusters will provide ready identification of cluster members and diffuse line emission associated with the clusters, as well as the ability to identify and obtain redshifts for background lensed objects.

In addition to measuring the clustering of galaxies, IFIRS is also ideally suited to identifying the sub-galactic fragments that, in hierarchical models, characterize the early stages of galaxy formation (Fig. 6). Recent studies with *HST* and Keck demonstrate that these fragments may be distributed over a large area (the entire IFIRS FOV) but form coherent structures with relatively small velocity dispersion (e.g., Pascarelle et al. 1996). Identifying

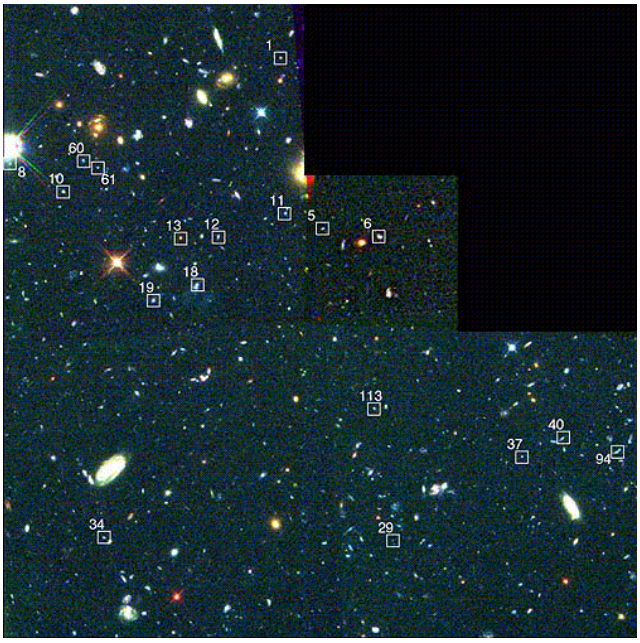


Figure 6: The boxes on this WFPC-2 image of the $z = 2.390$ radio galaxy 53W002 mark 18 candidate Lyman-$\alpha$ emission-line objects at $z \simeq 2.4$ which were identified on the basis of narrow-band imaging by Pascarelle et al (1996). Their proximity ($< 600/h$ kpc) and small velocity dispersion, ($\simeq 300$ km s$^{-1}$) has led to the claim that these fragments will merge to form an early type galaxy. Identifying all such fragments over the huge redshift column accessible to NGST with a conventional camera and spectrometer would require an extensive suite of narrow-band filters and follow-up MOS exposures. All such fragments would be found in a single IFIRS pointing.

all such fragments over the huge redshift column accessible to NGST, for even a single field, would be arduous without a large set of intermediate width filter observations combined with confirmatory MOS exposures. In contrast, all such fragments will be found in a single IFIRS scan. A subset of these fragments can be followed up at higher spectral resolution with the dispersed FTS mode in order to measure the velocity dispersion and internal kinematics of the fragments.

Finally, IFIRS can be used as an IFU to investigate the spatially resolved structures in galaxies near and far. At high redshift, the low resolution IFIRS surveys will result in spatially resolved (3D) spectroscopy for all $\simeq 10^4$ galaxies in a deep exposure. No object selection will be necessary and separating the spectra of spatially overlapping sources (e.g., foreground objects overlying background objects) can be accomplished through deconvolution in the image plane. At low redshift, low resolution IFIRS studies can probe the spatial variation in the stellar content of large nearby galaxies (e.g., M 51). Higher resolution IFIRS scans in strategic narrow filters will probe the dynamical, chemical and structural properties of these galaxies.

### 2.1.2 First Light & the Epoch of Reionization

The core mission of NGST is focussed on investigating the end of the dark ages and the formation of the first galaxies. Our present understanding of this epoch ($z \sim 10 - 30$, <1 Gyr

from the Big Bang) is speculative (current observations barely extend beyond $z \approx 5$; e.g., Dey et al. 1998), but it is during this era that matter was transformed from the smooth distribution reflected in the cosmic microwave background radiation to the highly clumped one observed today. Also during this age, the first luminous objects shone forth, reionizing the universe. The detection of the first luminous objects and the determination of the redshift of reionization therefore provide effective discriminants between competing theories of structure formation (e.g., Loeb 1998).

Fig. 3 shows the number of faint galaxies per IFIRS field of view and indicates the $SNR = 10$ threshold for deep exposures ($10^5$ s) at $R = 1$, 5, & 100 at $K$. At $K \leq 27.5$ AB mag there are 10,000 objects per IFIRS field of view; low resolution ($R = 100$) spectra can be obtained for all of these objects. At this flux level Haiman & Loeb (1998) predict that there will be $30 - 10^3$ star forming clusters at $z > 5$, and $\lesssim 10$ with $z > 10$. The uncertainty stems from the star formation efficiency; if the fraction of gas converted into stars at this epoch is required to reproduce the C/H abundance ratio in the intergalactic medium at $z \simeq 3$ inferred from the Ly$\alpha$ forest, then numbers in the upper range are expected. Bright, high-$z$, proto-galactic clumps are the proverbial needle-in-a-haystack; the full field spectroscopic cabability of IFIRS can find these very rare objects which correspond to $< 0.1$ % of the faint galaxy population. Fainter clusters are likely to be more common; at nJy levels NGST might detect $3000 - 30,000$ clusters at $z > 5$ and $30 - 3000$ at $z > 10$.

Once these distant star-clusters, galaxies, or quasars have been identified, their spectra may be coadded to construct a very high signal-to-noise ratio composite spectrum that is a sensitive probe of the reionization epoch. Rather than hoping to find a single bright target in the dark ages, composite spectra may be the most reliable way to search for the reionization epoch: the luminosities and masses of the first collapsed objects are unknown, and there are likely to be many more small (faint) ones than large (bright) ones. As an additional efficiency factor, the imaging and spectroscopic data needed for this project can be obtained from the same IFIRS scans that were used to study the evolution of galaxies and the growth of structure (see previous section). Thus, if IFIRS is used for this experiment no additional observing time is needed to complete this project.

## 2.2 Cosmology

### 2.2.1 SN Cosmology

As an example of the rapidly changing face of astronomy, two teams recently reported plausible evidence that the expansion of the universe is accelerating (Schmidt et al. 1998; Garnavich et al. 1998ab; Perlmutter et al. 1998; Riess et al. 1998 Perlmutter et al 1999). This result, based on the Hubble diagram for type Ia supernovae (SNe Ia), implies the existence of a form of vacuum energy that drives the expansion, makes the large-scale geometry Euclidean, and contains most of the energy density in the universe. Grand unified theories can easily accomodate a value of zero for the true vacuum energy density. While a value of zero might have been expected for the symmetric vacuum in which the Higgs fields have zero magnitude, these astronomical observations may indicate that a broken-symmetric state describes our present universe, a state with non-zero values for the Higgs fields. Our inability to explain the extreme smallness of the cosmological constant is regarded by many particle theorists as one of the most important problems in physics (Steinhardt 1997). Consequently, if confirmed, an

astronomical detection of the cosmological constant would have tremendous impact on the field of fundamental physics. Hence, it is crucial to test this result through precise measurements of the cosmological parameters from the SNe Ia Hubble diagram.

IFIRS presents numerous advantages for NGST studies of high-$z$ SNe that are needed to distinguish between purely cosmological effects and systematic errors due to evolutionary effects (e.g., Kirshner 1999). With the broad free spectral range of IFIRS, we will be able to discover and study SNe at $z \gtrsim 1-5$ with the familiar rest-frame optical diagnostics on which our current understanding of SNe Ia is based. In order to test and employ SNe Ia as standard candles, the accurate and precise spectrophotometric calibration provided by an IFTS is critical. Broad-band spectrophotometry with IFIRS is necessary to establish the extinction from reddening along the line of sight to distant SNe and to determine, thereby, the extinction curve for cosmic dust as a function of redshift. Most importantly, the highly multiplexed MOS of IFIRS offers an unconventional but efficient approach to finding and studying large numbers of SNe.

In a traditional SN search, multiple epochs of imaging are used to select candidates on the basis of their variability. These are then scheduled for prompt spectroscopic followup, an inefficient and expensive process since $\lesssim 50\%$ of variable objects turn out to be SNe Ia (A. Riess, personal communication). The optimization of IFIRS for low resolution ($R \simeq 100$) spectrophotometry allows us to find and study SNe spectroscopically in a single visit. Simulated IFIRS data (figure 4) show that in a $10^5$ s, $R = 100$ exposure we can identify, classify, and measure the redshift of SNe to $z \simeq 5$ purely on the basis of their spectra. At a limiting flux of 35 nJy, about 24 SNe will be detected, $\simeq 30\%$ of which will be SNe Ia (Dahlen & Fransson 1998).

Because science can be spatially multiplexed with IFIRS, the SN search can be carried out in parallel with other NGST programs that call for deep ($t \simeq 10^5$ s), low resolution ($R \simeq 100$), $1-5$ $\mu$m imaging ($\simeq 10\%$ of the DRM). Over the 5-year NGST lifetime, these observations will yield, as a by-product, a catalog of about 4400 SNe, including about 1300 SNe Ia, with $\langle z \rangle \simeq 1.5$. With this serendipitous catalog, we will determine the rates at which SNe occur to $z \simeq 5$. The SN catalog can also be used to place constraints on the star formation history and IMF in the early universe, and the SNe Ia progenitor population.

Those SNe Ia discovered on the rising portion of the light curve ($\simeq 5\%$ of the SNe Ia in each data cube) can be scheduled for photometric monitoring in order to establish whether or not SNe Ia are standard candles (through a comparison of spectra and light curves). This program could be conveniently combined with the ultra-deep survey proposed in the galaxy evolution DRM. The multiple visits required to accumulate the necessary integration time could be distributed to provide light curve coverage for a hundred or so SNe Ia.

Alternatively, it is possible to determine the age of SNe Ia from their spectra and thereby extrapolate the apparent magnitude at maximum light by extrapolation from a single epoch by using a template light curve (Riess et al. 1998). In this scheme, no repeat images or spectra would be needed because single epoch observations are sufficient to compile a statistically significant Hubble diagram.

### 2.2.2 Gravitational Lensing

Large scale mass inhomogeneities along the line of sight distort both the apparent brightness and shape of distant objects. The latter effect being sensitive to all (luminous and dark) matter

along the line of sight, can, in the weak lensing limit, be used to make the link between the observed luminous universe and structure formation theories which can reliably predict the distribution of dark matter.

As demonstrated by HST, deep, high angular resolution imaging such as that provided by IFIRS is critical in lensing studies (e.g., Kneib et al 96; Smail et al 96; Seitz et al. 96). With IFIRS, lensing studies would be carried out at low spectral resolution ($R = 5$), where the background lensed galaxies are selected on the basis of photometric redshifts, and shear parameters are measured from the deep panchromatic image. Since the $SNR$ of the lensing shear signal is $SNR_{shear} \propto \sqrt{n}/\sigma_\epsilon$, where $n$ is the number of galaxies with measured ellipticity and $\sigma_\epsilon$ is the width of the intrinsic ellipticity distribution (Schneider P., & Kneib, J.-P. 1998 astro-ph/9807091), the large field of view of IFIRS means that a large number of galaxies can be studied in a single pointing, resulting in a significant speed advantage.

A more significant advantage is the use of the IFIRS deep panchromatic image to measure the ellipticity of faint galaxies. If IFIRS and a filter camera were both used to conduct a $JHKLM$ lensing survey, then the IFIRS panchromatic image, i.e., the image formed by summing the 1-5 $\mu$m signal, has a $\sqrt{5}$ $SNR$ advantage compared to the camera. This factors directly into an increase in $SNR_{shear}$. This is a significant advantage because image morphology and not color information is the limiting factor for measuring lensing. Use of the panchromatic image to measure image parameters is justified by Dickinson et al. (1999) who have shown that in the NICMOS HDF the morphology of faint galaxies through 1.6 $\mu$m shows remarkably little variation with wavelength. Thus the combination of field of view (a factor of 1.75) and the deep pan-chromatic image (a factor of 5) yield a total speed gain of 8.7 over the ISIM yardstick.

Since SNe have well-defined photometric properties and light curves, the possibility of detecting lensed SNe in the IFIRS serendipitous catalog suggests some ingenious experiments. For example, the measurement of the time delay between multiple images of lensed SNe offers a powerful method of determining $H_0$. The use of gravitational lenses, in general, for determining $H_0$ is advantageous because it provides a single-step measurement of $H_0$ for each system and avoids the propagation of errors along the distance ladder. While lensed quasars have typically been used in this approach, they suffer from the correlated $1/f$-noise that dominates quasar brightness fluctuations. The correlated noise produces a broad peak in the cross-correlation of the light curves of the different images, making it difficult to precisely measure the time delay. In contrast, lensed SNe have a well behaved light curve, making it possible to establish the time delay to within a few days. As an additional example, mass estimates for clusters obtained from weak lensing studies are uncertain by a constant of integration. If the lensed source is a standard candle, such as SN Ia, the absolute magnification can be determined and used to break the mass sheet degeneracy, allowing an estimate of the total cluster mass (Schneider & Seitz 1995).

## 2.3 Star and Planet Formation

The unprecedented sensitivity of NGST at thermal infrared wavelengths makes it a powerful tool for studies of star and planet formation and for observations of brown dwarfs and extrasolar planets. NGST will provide the power to peer into the central regions of the youngest protostars to study the processes by which stars are assembled from molecular cloud cores

and the speed to study large samples of planet forming systems to understand when and how planetary systems are created.

Many star and planet formation studies will require large spectral samples and broad wavelength coverage, needs that are well matched to the capabilities of IFIRS. For example, NGST will have a tremendous impact on the study of protoplanetary disk evolution. For this program, large samples are needed to understand how disk evolution depends on age, stellar mass, binarity, and environment. Clusters are ideal targets for such studies because they contain many stars over a narrow range in age, and can thereby provide statistically significant samples as a function of stellar mass and binary separation. The low- to moderate-resolution ($R = 5 - 1000$) spectroscopy provided by IFIRS at $1 - 28$ $\mu$m is optimal for studies of disk dust and gas. This wavelength range will probe the properties of disks from the inner disk edge out to planet forming distances ($\sim$ few AU). The tremendous sensitivity of NGST shortward of 28 $\mu$m, when combined with the spatial multiplexing capability and large field of view of IFIRS, will make it possible to obtain complete spectroscopic surveys of young star clusters at distances beyond 1 kpc.

With the unique ability to reach such distant regions, we will be able to study both rich clusters and clusters in the critical age range $5 - 30$ Myr. Disks are believed to disperse sometime within this age range, and a precise measurement of the disk dispersal time, refined from the study of large samples, would constrain the timescale for terrestrial planet formation. With the high angular resolution imaging capability ($0.''3$ at 12 $\mu$m) of IFIRS, we will be able to resolve crowded stellar fields in these distant clusters, as well as diagnose and study binarity in nearby star forming regions. Close binary companions are expected to significantly impact the likelihood of planetary formation in disks by altering disk structure and disk dispersal time. These effects can be studied with IFIRS broad-band imaging and low resolution spectroscopy. Spectroscopic studies of both crowded fields and close binaries will benefit from our ability to carry out spectral deconvolution in the image plane with IFIRS imaging spectroscopy.

More specifically, low resolution spectroscopy ($R \simeq 20 - 100$) will probe radial disk structure, revealing gaps that indicate the presence of young protoplanets. These measurements require precise spectrophotometry over an extremely large wavelength range ($1 - 28$ $\mu$m; e.g., Carr & Najita 1998), such as that provided by IFIRS. The large samples studied by IFIRS will enable robust statistical comparisons between protoplanet frequency and the frequency of giant planets around older main-sequence stars. We will thereby probe directly the role of dynamical evolution in planetary systems, heretofore unexplored territory. The evolution of gas in the inner planet forming regions of disks is another critical question that can be answered by IFIRS. Studies of the evolution of gas in disks not only enable more direct measurements of disk mass and its evolution with time, but can also measure the timescale for giant planet formation. IFIRS measurements of the MIR rotational $H_2$ lines in large samples of young stellar systems will measure the gas dissipation timescale.

An analysis of the ability of IFIRS to carry out the $H_2$ survey portion of the DRM proposal on the Evolution of Circumstellar Disks illustrates the speed advantage of carrying out this and similar surveys with an IFTS. The proposal envisions targeting 120 stars, observed one at a time with a cross-dispersed MIR spectrograph in order to measure the disk $H_2$ content. However, after the sample is divided into even only 12 bins based on age, stellar mass, and clustering environment, it is clear that 120 stars is completely inadequate to understand the dependence of gas content on these quantities, especially since other variables such as binarity,

inclination effects, and intrinsic variation are not considered. In comparison, with ($R \simeq 1000$) FTS scans through narrow-band filters centered on the MIR rotational $H_2$ lines, in just 5 days, IFIRS could observe four $5 - 30$ Myr old clusters beyond 1 kpc and at least 8 star-forming clusters (age $< 10$ Myr) within 1 kpc. Assuming a modest 300 stars per field of view, the final sample is nearly 4000 systems. In contrast, the original DRM requested triple the time (15 days) to acquire similar data for only 120 systems. Compared to a slit spectrograph, IFIRS further improves this experiment by providing precise spectrophotometry of the line emission and improved subtraction of any extended $H_2$ emission.

As examples of the power of spatial multiplexing with IFIRS, $H_2$ spectral-imaging for the Disk DRM proposal will also measure $H_2$ emission in stellar jets, shocks, and photodissociation regions, thereby simultaneously accomplishing 35% of the Physics of Star Formation proposal and a reasonable fraction of the Interstellar Medium DRM proposal. In addition, while IFIRS is studying the properties of disks in distant young clusters, it can simultaneously measure the mass function of sub-stellar objects from brown dwarf to super-planet masses. The $R \simeq 100$ IFTS scans that will reveal the radial structure and dust content of disks will also probe the atmospheres of several hundred very low-mass stars and sub-stellar objects per cluster, e.g., via $H_2O$ and $CH_4$ bands. IFIRS can detect and study 10 Myr old free-floating super-planets of $5M_{Jup}$ at a distance of 1 kpc in $10^5$ s.

An exciting possible outcome of such studies is the discovery of extra-solar giant planets (EGPs) that have been ejected from young planetary systems. These planets can be distinguished from free-floating EGPs that formed in isolation by their high proper motions that will far exceed the velocity dispersions in young clusters. Due to the large IFIRS field of view, there is a high probability of discovering ejected EGPs. Ejected EGPs will provide an unique opportunity to study, via $R \simeq 100$ spectroscopy, the atmospheres of true Jupiter analogs (i.e., planets with a formation history similar to that of our own solar system) without the usual difficulties of studying orbiting planets in the glare of the central star.

### 2.3.1 Ecliptic Plane Surveys

Studies of the ecliptic plane, and the Kuiper Belt in particular, are critical to our understanding of the formation and evolution of the solar system, both as the source of short period comets and as the best preserved clues to the conditions in the solar system during the epoch of planet formation. Spectroscopic studies of moving objects such as planets and Kuiper Belt objects (KBOs) present no intrinsic difficulties for an IFTS since the interferogram for a moving source can be formed by registering and stacking the series of short individual exposures. IFIRS will be able to obtain the deepest census of Kuiper Belt objects, mapping its population and dynamical structure. The unparalleled sensitivity of NGST will permit deep searches (to $K = 31.4$) which should yield photometry for about 100 new objects per IFIRS field. While broad-band colors (dominated by reflected light) are only weakly diagnostic of composition (Clark 1982), IFIRS low resolution ($R = 100$) spectroscopy of the brighter KBOs ($K < 27.5$) will be able to detect and study absorption features produced by ices (e.g., $H_2O$, $CO_2$, $N_2$, $NH_3$, $CH_4$), the likely major surface constituents of KBOs.

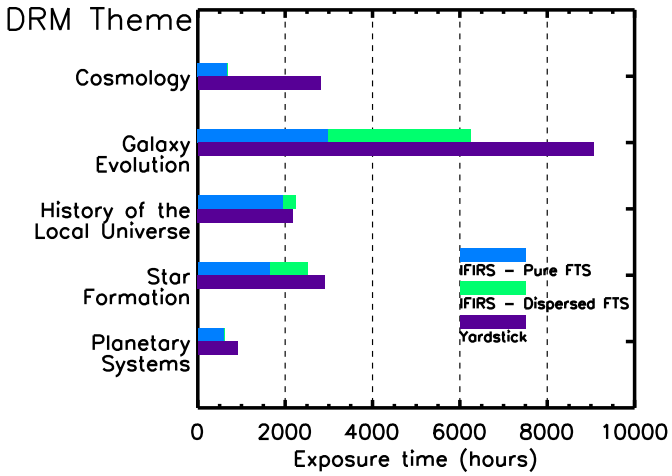


Figure 7: A comparison of the integration time required to complete each DRM theme using IFIRS and the Yardstick ISIM. The breakdown between pure FTS ($R < 300$) and dispersed FTS ($R > 300$) is shown.

## 2.4 IFIRS and Design Reference Mission

To provide a quantitative evaluation of the performance of IFIRS we have calculated the exposure time required to perform the NGST DRM. The results are listed in Table 2 and displayed in Fig. 7. The input file was the configured Ad Hoc Science Working Group science program version 2.1, dated July 28, 1999.[3] For comparison, and as a consistency check, we also tabulate the results that our spread sheet predicts for the Goddard Yardstick ISIM. The Yardstick telescope and spacecraft are assumed for all calculations. We conclude that IFIRS can perform the entire DRM and in only 69% of the time required by the Yardstick ISIM. This is remarkable, since the DRM was designed around the Yardstick instruments, i.e., traditional cameras and spectrometers. These calculations reflect the execution of the DRM in the manner imagined by the authors of the programs, except where the use of the IFTS panchromatic image is advantageous. The speed advantage of IFIRS can be traced to two factors: 1) a 10% reduction in total exposure time from use of the panchromatic image to combine imaging and spectroscopy; 2) an additional 20% reduction in exposure time due to the large IFIRS field of view. As shown in Fig. 7, the pure FTS mode represents the majority (64%) of the DRM exposure time.

The above analysis neglects the huge potential multiplex advantage with the IFTS, i.e., a single set of IFIRS surveys can accomplish much of the core NGST mission. For example, consider an IFIRS $10^5$ s deep field survey carried out over $1-5$ $\mu$m at a resolution of $R = 100$. The panchromatic image constructed from the survey can be effectively used to investigate weak lensing in the faint galaxy population and the morphologies of the faintest galaxies. The low resolution spectroscopy will yield $SNR > 10$ spectra for all objects with flux densities >35 nJy. At this flux density limit, we expect 10,000 galaxies, 100 $z > 5$ quasars, 300 high-$z$ proto starclusters, and 24 SNe per pointing. This single observation can therefore be used to investigate the clustering properties of the field galaxies; identify the highest redshift populations; discover the first light objects and study their spatial and redshift distributions;

[3] http://www.ngst.stsci.edu/nms/main/

Table 2: **DRM Exposure Time Requirements**

| DRM Theme | IFIRS (hours) | Yardstick (hours) |
|---|---|---|
| Cosmology | 689 | 2810 |
| Galaxy Evolution | 6244 | 9063 |
| History of the Local Universe | 2242 | 2175 |
| Star Formation | 2521 | 2911 |
| Planetary Systems | 612 | 907 |
| Totals | 12307 | 17866 |

study the spatial variations in star-formation rate and dust extinction in the extended galaxies; identify gravitational arcs or other strong lenses; identify all transient objects, and thus type, age-date, and provide accurate spectrophotometry for all SNe; provide a composite high-redshift spectrum to determine the redshift of reionization.

Deep ($10^5$s, $R = 100$) surveys of the ecliptic plane, in addition to revealing new members of the Kuiper Belt, will also probe the properties of faint halo stars and distant galaxies. Given the broad wavelength coverage of IFIRS, much of the science in the star and planet formation DRM proposals can also be carried out simultaneously. For example, wide-field $H_2$ emission line measurements in star forming regions and young clusters could be used to study emission from disks, jets, and protostars. IFIRS low resolution MIR spectroscopy of rare embedded protostars would simultaneously probe the circumstellar disk structure of hundreds of the more populous older stars in the same clusters. Similarly, IFIRS low resolution NIR spectroscopy ($R = 100$) of cluster stars to study the properties and initial mass function of low mass stellar and sub-stellar objects will simultaneously probe the inner disk properties of hundreds of stars.

Hence, if the DRM was re-designed to take maximal advantage of the capabilities of IFIRS (e.g., simultaneous imaging and spectroscopy, spatial multiplexing, broad wavelength coverage), a considerable savings in total exposure time would be achieved. Perhaps more significantly, since IFIRS acquires a spectrum for every pixel in the field of view, it would simultaneously collect additional scientifically useful data *beyond* that specifically called for in the DRM. Programs designed around the capabilities of IFIRS are, thus, likely to achieve a scientific output well beyond the scope that can be envisioned or implemented with traditional instrumentation.

# 3 ENGINEERING

## 3.1 Summary

IFIRS provides, in a single instrument, the capability to fulfill the requirements of the NGST DRM, the needs of the target acquisition and fine guiding sensors, as well as the high quality imagery necessary for measurement and control of the wavefront error (WFE) of the optical

telescope assembly (OTA). IFIRS delivers the diffraction-limited performance of a conventional camera, while at the same time providing the high spectral resolution and sensitivity of a multi-object spectrometer. In addition, some types of observations which are not practical with slit spectrometers, such as spectroscopy of moving objects (e.g., planetary targets) may be made by registering and stacking the sequence of interferograms.

The philosophy of the IFIRS point design was to enable the acquisition of all components of the DRM with greatest efficiency. The choice of an IFTS architecture emerged because of its ability to perform the DRM science, while maintaining the greatest practical efficiency, sensitivity and flexibility; and at the same time reduce program risk by minimizing reliance on technology development. The flexibility to be configured on orbit, to adapt to the spectral resolution needs of observations a decade from now (which may well be different than currently envisioned), as well as the desire to obtain a spectrum for every pixel, were given great weight. Indeed, such unbiased acquisition of spectral information maximizes the possibility for fortuitous discoveries of the unknown and the unexpected.

The IFIRS baseline design concept exploits the fact that an imaging Michelson interferometer provides simultaneously both broad-band conventional imaging as well as arbitrarily variable resolution spectroscopy (up to a designed maximum, and subject to appropriate sensitivity limits) for every pixel in the field of view of the imager. The loss relative to a generic camera having relay optics similar to the IFIRS collimator and objective is negligible: two beam splitter encounters (99% each), and three cube-corner reflections (99% each), totaling approximately 5% loss. There are three options for imaging: 1) at any OPD the two output ports can be summed to obtain an unmodulated image; 2) the interferometer may be held at zero path difference (ZPD), and only one FPA is readout; 3) no beam-splitter is selected, and again only one is readout. For simultaneous imaging and spectroscopy the sum of the two output ports produces imaging data of quality equal to that of a conventional camera. The few percent loss of throughput due to the beam splitter is more than made up for by the gain in scientific throughput provided by the simultaneously acquired spectral information. It is unnecessary, for example, to choose between a near-IR camera observation or a near-IR spectroscopic observation. The camera-like signal levels at the FPA, for moderate spectral resolution observations ($R < 300$), implies that with the current level of NGST near-IR de-

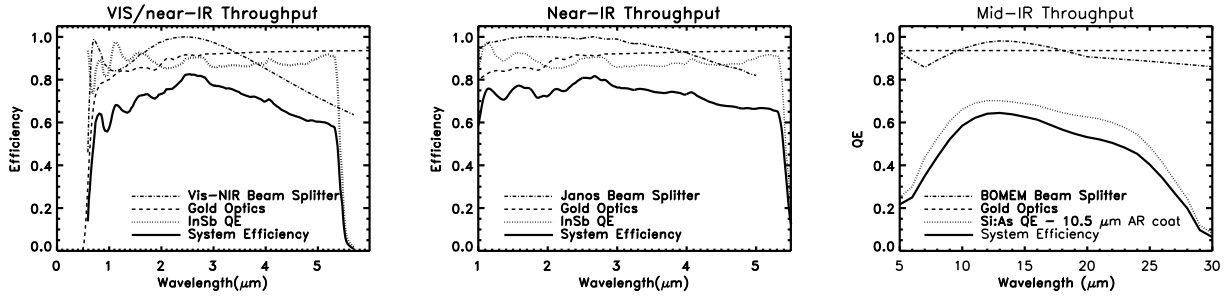


Figure 8: The throughput of IFIRS for the visible, near-, and mid-IR. Visible and near-IR observations use the same detector but two different beam-splitters. The short wave sensitivity is limited by the choice of gold as the mirror coating. The mid-IR detector AR coating is optimized for 10.5 $\mu$m, which determines the short wavelength performance of this channel. These plots do not include the OTA.

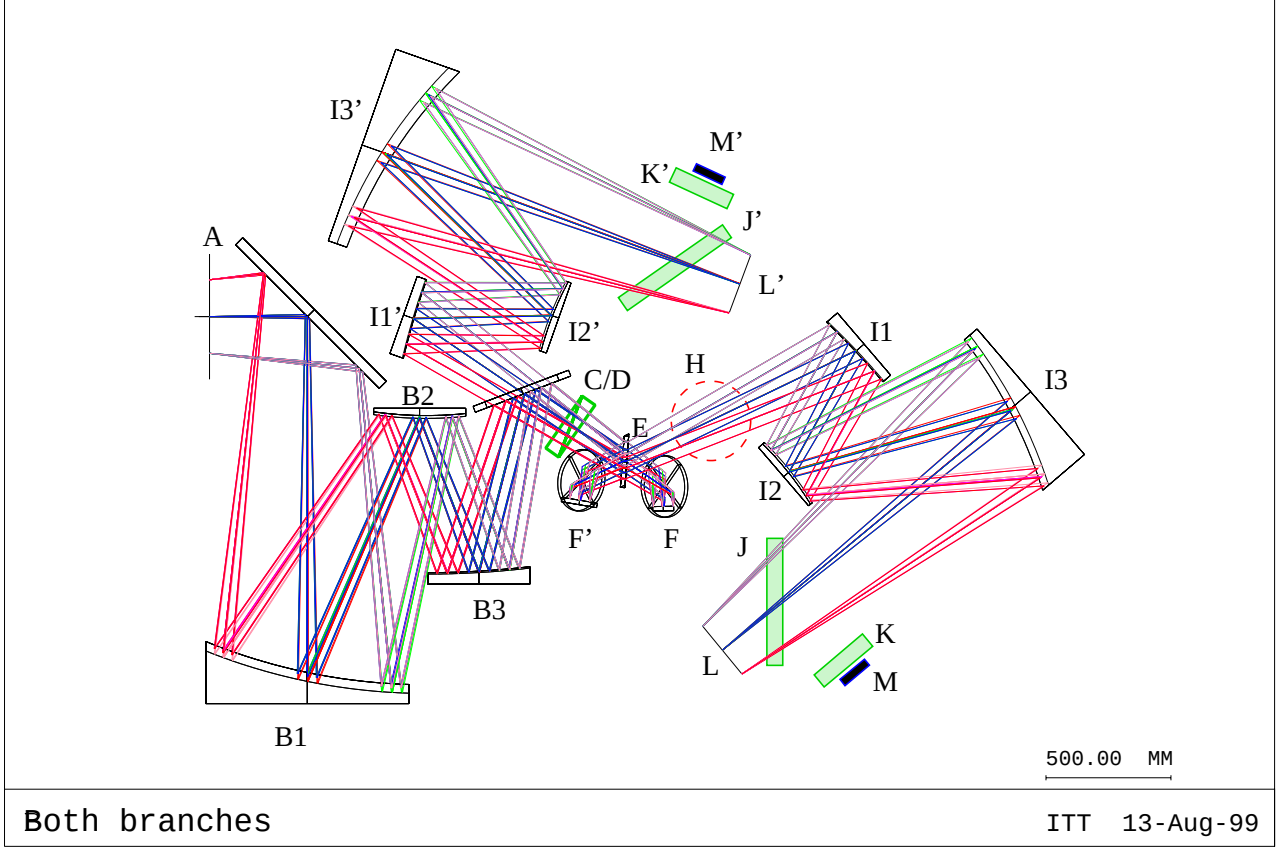


Figure 9: A plan view of the IFIRS optical layout generated from the CODE V optical prescription. A) the OTA focal plane, B) collimator TMA; C/D) selectable blocking filter and prism assembly; E/F) the interferometer beam splitter and cube corners; H) Calibration sphere; I) the camera TMA; J) selectable fold mirror; K) mid-IR blocking filter; L/M) the near- and mid-IR focal plane arrays. Primes refer to the components in the second output port. The moving mirror actuator, labeled G in Fig. 10 is not shown.

tector performance, zodiacal limited performance can be easily achieved. The overall system efficiency for converting incident photons from the OTA to photoelectrons is shown in Fig. 8.

Furthermore, by simultaneously obtaining imagery with spectroscopy, multiple science objectives may be met by a single observation, and thus very efficient parallel acquisitions may be made. Finally, with the addition of an programmable image plane aperture mask and a prism in collimated space, even the high spectral resolution domain ($600 < R < 10,000$) may be obtained with IFIRS at sensitivities equivalent to a dedicated dispersive spectrometer.

## 3.2 The IFIRS Design Concept

The IFIRS instrument, displayed in Fig. 9 in plan view and in Fig. 10 in solid body view, consists of the following elements, listed approximately in order of encounter with starlight. We assume that the interface to the OTA begins at an appropriate image plane or aperture mask, which we have further assumed to be a selectable, programmable, micro-shutter array:

**A.** A selectable aperture mask located at the image plane of the OTA. Normally, this mask is removed from the optical path. For observations using the dispersed FTS mode this aperture mask is configured to transmit light for small regions surrounding each object. This enables efficient observations at the highest spectral resolution ($R = 600 - 10,000$) over the full $5'.3 \times 5'.3$ IFIRS field. For coronagraphic observations, a special aperture mask is used to block light from the central object.

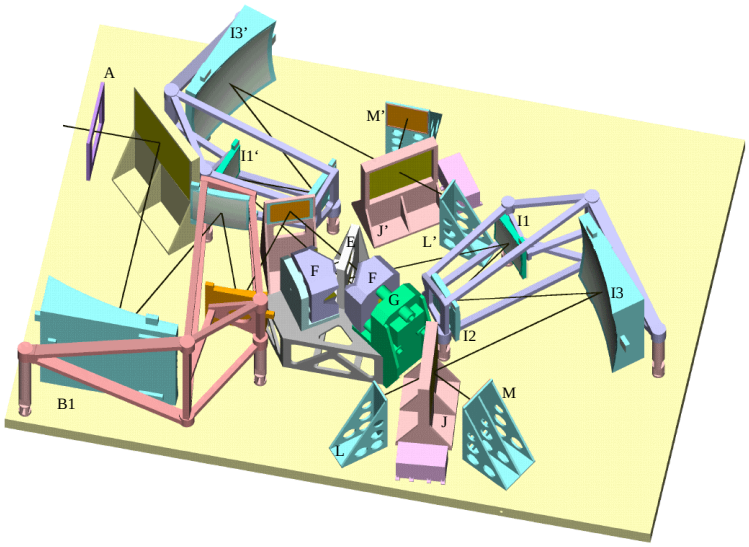


Figure 10: The solid body model of IFIRS. Labels are the same as in Fig. 9. G is the OPD drive. This figure illustrates the spatial separtion between the input and output rays. The input enters on the upper deck of the interferometer, and exits on the lower deck.

**B.** A three mirror anastigmat (TMA) collimator. This produces an image of the OTA pupil in the center of the downstream interferometer (E/F). The surfaces are gold coated, which produce the maximum efficiency for the IR, at the sacrifice of some efficiency at $\lambda < 0.6$ $\mu$m. The imaging performance of the IFIRS optical system, [4], including both the collimating and the re-imaging TMA's, is demonstrated by the set of spot diagrams in Fig. 11. A wavefront error budget tree is displayed in Fig. 11.

**C.** A selectable prism assembly, only used in the dispersed FTS mode for obtaining the highest spectral resolution observations. A suite of anti-reflection (AR) coated Zenger prisms are used to cover the full NGST wavelength range in three sections, 0.6-3.4 $\mu$m (Sapphire/KCl), 0.96-5.4 $\mu$m (also Sapphire/KCl, but AR coated for 1-5$\mu$m), and 5-28 $\mu$m (CsI/CsBr AR coated for 6-18 $\mu$m). For each prism pair, the central color passes through undeviated, while the average resolution is $R \simeq 600$. The prism is used in conjunction with the aperture mask to enable the highest practical sensitivity at high spectral resolution ($600 < R < 10,000$). In this mode, the interferometer produces high resolution spectra within the small bandpass corresponding to the prism dispersion over the width of a pixel. The wavelength calibration is precisely determined by the metrology laser. A large gain in sensitivity over the non-dispersed mode is obtained (at the expense of full field imaging) by virtue of the lower integrated noise bandwidth seen by any given pixel. Dispersion by prism rather than by grating enables higher efficiency over a broad band-pass, as shown in Fig. 12.

**D.** A selectable bandpass limiting filter, used for spectrally targeted observations and mutually exclusive to the Zenger prism. This filter is located upstream of the interferometer in order to assure that the spectral range seen by the two output ports is the same. For example, if a $K$ filter is used, the IFIRS panchromatic output yields a regular $K$ image with the sensitivity of an ordinary camera, while at the same time spectroscopy from 2.0-2.4 $\mu$m at the commanded spectral resolution is obtained for all pixels in the field of view. For

[4]The optical prescription for the entire imaging system is available at http://astro.berkeley.edu/~jrg/ngst/optics.html.

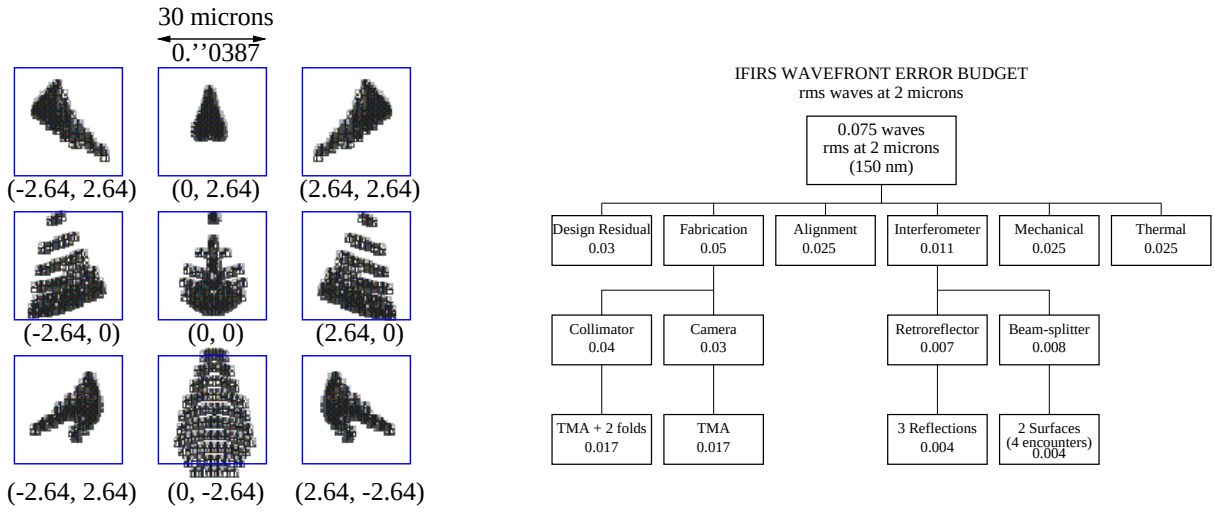


Figure 11: **Left:** Polychromatic (1, 3, & 5 $\mu$m) spot diagrams illustrating the image quality over the full IFIRS field of view. Field points are labeled in arc minutes. The boxes represent the size of the near-IR 30 $\mu$m pixels. There is no significant dependence of the geometrical imaging with wavelength. **Right:** The IFIRS wavefront error budget tree, displaying the allocation of error terms to the various components that are added in quadrature to produce the final rms WFE of 0.075 waves (rms) at 2 $\mu$m and a Strehl ratio of 0.8. The tight tolerance allocated to the interferometer ensures that high modulation efficiency may be obtained for interference between the two beams.

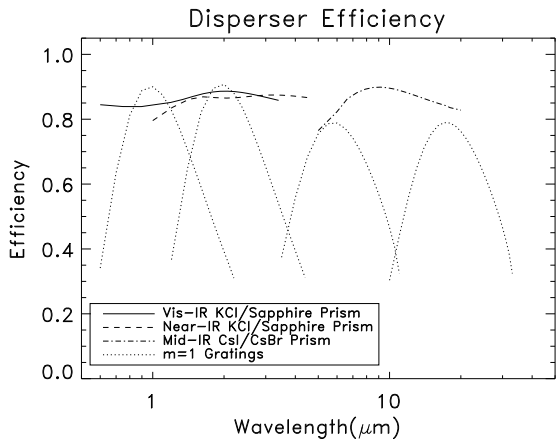


Figure 12: A comparison of prism efficiency with grating efficiency as a function of wavelength. The vis-IR and near-IR prisms consist of $KCl/Al_2O_3$ and the mid-IR prism is CsI/CsBr. For comparison the efficiency of gratings blazed at 1, 2, 6, & 20 $\mu$m used in first order are shown. For the spectral range $0.6 - 20$ $\mu$m, it is necessary to use at least 4 separate gratings.

observations not targeted to a particular spectral range, the band-limiting filter is removed, and the interferometer is used to synthesize the required set of band-passes, e.g., $RIJHKLM$. In this case, the IFIRS panchromatic output enables very deep imaging over a spectral range determined by the sensitivity of the detector array. For InSb, this corresponds to 0.6-5.6 $\mu$m, while for Si:As this corresponds to 5-28 $\mu$m.

**E, F, & G.** A Michelson 4-port interferometer, with a selectable beam-splitter (E). The two output ports feed identical reimaging systems, which produce complementary images at their FPAs. One input port is fed from the OTA, while the other input port is fed from a calibration source/cold-load (H). The input ports lie in an upper plane, while the output ports lie in a lower plane. The final processed interferogram is constructed from the difference between the two outputs, and is therefore immune to common mode noise, e.g., a variable background, while the normalized fringe visibility ratio is invariant to gain changes, e.g., variable throughput.

Beam-splitters cover the wavelength range in three sections, 0.6-3.4 $\mu$m, 0.96-5.4 $\mu$m, and 2-28 $\mu$m. Modulation efficiency curves for these three spectral ranges are displayed in Fig. 8. The modulation efficiency is a factor in the spectrally resolved data, but only the system transmission efficiency matters for panchromatic imagery. The interferometer mirrors (F) are cube corners, which follow the "aligned by design" paradigm. The OPD in the interferometer is manipulated using a cryogenic actuator (G).

For a typical observation, the OPD is stepped to a specified position under active laser metrology control, and then held in place, with the metrology laser turned off. During the science observation, capacitive displacement sensors are used to control the OPD. The laser metrology system, not shown in the optical layout, feeds laser light to the beam-splitter along a plane midway between the infrared incident and exit beams. The split laser beams are retro-reflected from near the vertices of the cube corner mirrors, returning along the midplane, to be recombined at the beam splitter. Phase quadrature detectors determine the phase of the metrology laser interference fringes to measure the OPD separation within a laser wavelength, while an up-down counter keeps track of the total number of laser phase cycles with respect to ZPD. Having the laser on only during OPD steps enables very high bandwidth, high intensity laser metrology for the absolute determination of OPD over a very large OPD range, yet does not produce a stray light background problem for the low science light levels. The minimum step size is limited only by the precision of the phase quadrature measurement (0.6 nm), while the maximum OPD is 10 mm, to allow for resolution values up to $R = 10,000$ at 1 $\mu$m.

**H.** A calibration system which feeds the second input of the interferometer. The primary input port is blanked off and the second input port is illuminated, enabling comprehensive calibration of pixel-to-pixel gain and offset, and the overall spectral response and efficiency. The calibration light is obtained from one of a set of optical fibers, which are mounted on the sun-lit side of the spacecraft at their input end, and feed an integrating sphere at their output end. The fiber diameter and transmissions are adjusted to allow for light levels comparable to those characteristic of the science observations. The selection of the active fiber is made at the entrance end, in warm space, in order to avoid dumping extraneous heat or light into the cold science instrument package. For science observations, all of the fibers are blocked at the input, and the integrating sphere is held at the ISIM box temperature. The exit aperture of the integrating sphere faces the second input port of the interferometer.

**I.** A pair of TMA cameras, one for each output port. These produce a final image of the

scene at the detector arrays.

**J.** A selectable fold mirror that is removed for Vis/near-IR observations and is inserted to direct light towards the mid-IR detector arrays for 5-28 $\mu$m observations.

**K.** A selectable, cold (6 K) bandpass filter set, in the path to both of the mid-IR detectors, but neither of the near-IR detectors, which enables restriction of the transmitted spectral range to the mid-IR detectors and thereby control the internal instrument background which reaches these detectors. Since the GSFC ISIM thermal interfaces are at 6 and 25 K, we have chosen to restrict the wavelengths reaching the mid-IR FPA rather than cool the entire TMA assembly to 6 K. This ensures that the long wavelength performance is only limited by scattered thermal (90 K) radiation from the sun-shield. Important mid-IR bandpass filters include: a $\lambda > 12$ $\mu$m blocking filter for zodiacal background limited observations, and a $\lambda > 25$ $\mu$m blocking filter for sun-shield limited observations. It is desirable to match the transmission characteristics of these blocking filters in order to suppress common mode noise.

**L, M.** The near-IR detector array system (L), an 8192 $\times$ 8192 InSb mosaic array of 30 $\mu$m pixels for 0.6-5.6 $\mu$m observations, and the mid-IR detector array (M), a 2048 $\times$ 2048 Si:As mosaic array of 60 $\mu$m pixels for 5-28 $\mu$m observations. From this point on, the IFIRS instrument has components essentially identical to an ordinary camera system, including a focusing mechanism to adjust for small mechanical distortions such as those produced by residual thermal gradients.

**N.** A ISIM thermal housing which maintains the 25 K environment for IFIRS as a whole and the 6 K cold head for the mid-IR detectors. This item is government furnished equipment (GFE).

**O.** A data acquisition and handling system (partially GFE), which digitizes the photocurrent levels, does the low level on-board processing, such as cosmic ray event mitigation, bad pixel fix-up, data compression, and temporary data storage prior to telemetry to earth. In order to maximize the efficacy of the data compression, an on-board calibration of pixel to pixel non-uniformities is made prior to down-link. In addition, correlations of successive interferogram samples for oversampled data are exploited to enable more efficient data compression, anomaly detection, and cosmic ray rejection.

**P.** In addition to the above items, IFIRS also includes the software to command and control the instrument, the thermal management system, the mechanical support structures, the launch lock down mechanisms, and the provision of IFIRS subsystem housekeeping data to the satellite.

### 3.2.1 Optics Design Description

The first two mirrors of the OTA resemble a Ritchey-Chrétien telescope and produce an internal image at f/15. Relay optics reimage the scene at f/24. It is this second image that is the input to the IFIRS instrument. With an 80 mm aperture exit pupil collimator at the center of the IFIRS interferometer, one has an afocal angular magnification of 100. The IFIRS design assumes a flat field at the f/24 image. The design requires at least one more iteration to account for the OTA's relayed image having a radius of curvature of about $-2.2$ m (Menzel 1999). This iteration should not have a major impact with the Wetherall-Womble type TMA. With this next iteration the entire system would have zero Petzval sum.

The FPA pixel sizes are assumed to be 30 and 60 $\mu$m for the near-IR and mid-IR bands respectively. The near-IR FPA is an 8192 $\times$ 8192 pixel array yielding a field of view of

$5'.28 \times 5'.28$. The 1:1.20 collimating and focusing elements together provide zero sum Petzval curvature terms so that the overall system is flat fielded. The image scales are $0.''0386$ and $0.''0772$ per pixel respectively for the near-IR and mid-IR bands and correspond to Nyquist sampling at 3 and 6 $\mu$m respectively. Relative to the diffraction limit, IFIRS is almost a factor of three times better sampled at $K$ than the WF chips of WFPC-2/*HST* at $R$.

The predicted optical performance is based upon the wavefront error budget shown in Fig. 11. This quality applies only to the f/24 and f/20 sub-apertures being employed by a given field point within the image. For the collimator optics and interferometer entrance fold mirror, these sub-apertures range from 53 mm to 100 mm. These sub-apertures also correspond to a linear range of 8% to 34% of the full aperture. In terms of area, the fractions range from 0.64% to 12%. To arrive at an adjusted rms OPD quality for the entire mirror, one needs to carry out a low frequency slope error analysis for each surface. First order peak-to-valley analysis leads to a slope error of about $1.3 \times 10^{-3}$ $\mu$m/mm. An astrometry specification relating to allowed mapping distortion in the final image must support this analysis. Optical design residual spot sizes at 1, 3, and 5 $\mu$m for the off-axis collimator and TMA anastigmat camera objective are shown in Fig. 11.

### 3.2.2 A Typical Observation Sequence

A typical observation scheme shows how IFIRS acquires data and gives an indication of the data transmission requirements. Consider, for example, a full field, near-IR measurement at $R = 6$, comparable to $IJHKLM$ measurements appropriate for photometric redshift determinations of distant galaxies. The telescope is pointed at the target field, and the $0.96 - 5.4$ $\mu$m beamsplitter and a 0.96 $\mu$m long pass filter are selected. The corresponding frequency range is $1850 - 10,400$ cm$^{-1}$. The aperture mask and the prism are not used. If needed, a check of the focus and targeting may be made by acquiring an image at ZPD and comparing the full intensity primary output to an uploaded finding chart. The OPD is stepped from -6857 to 6857 nm with respect to ZPD in 24 steps of 571 nm. The spectral resolution is approximately 1460 cm$^{-1}$, and 6 independent spectral channels are produced centered at 1.0, 1.2, 1.5, 1.9, 2.5, and 3.9 $\mu$m. By scanning symmetrically about ZPD the need for a phase calibration is eliminated, and each OPD is measured twice to permit dithering and to assist in vetoing cosmic ray events which escape on-board processing. The integration time weighting at each OPD is determined by the required spectral line shape function (cf. Bennett 2000). A uniform weighting produces a *sinc* spectral response function; a Gaussian weighting produces spectral channels with a Gaussian response.

The overhead for moving the interferometer OPD is less than the 10 s for reading the arrays. The integration time at each OPD step is typically a few hundred seconds and typically $< 800$ s to minimize the number of cosmic ray hits per frame. The time to acquire a full deep data cube is about 5 hours. The outputs of the individual FPAs composing the 8K$\times$8K system are multiplexed onto 32 output lines so that 67 Mpixels/32 lines $\times$ 5 $\mu$s/pix=10.5 sec. The rate of 5 $\mu$s per pixel is conservative and leads to a low power dissipation. For bright objects which require integration times $< 10$ s, a subarray of the FPA can be read out.

After the interferometer is moved to a new OPD the FPAs are reset and then continuously read every 10 s without resetting to measure the photocurrent. If a cosmic ray hit deposits insufficient charge to saturate a pixel, the slope on either side of the hit is averaged. If a cosmic ray hit saturates the pixel, the photocurrent prior to saturation is recorded as the

signal. Because the entire band is integrated on the pixel, the frame time to fill a pixel is shorter than with a camera (by approximately a factor equal to the resolution, i.e., $\simeq 10$ in this example), and much less than for a dispersive spectrometer, and the likelihood of a significant cosmic ray hit during a frame read also less. The calculation of the photocurrents implies a floor on the on-board memory requirements of the instrument processor. At minimum, if 4 words per pixel are required for 134 Mpixels to calculate a running average of the photocurrent at each OPD step (the current sample, the previous sample, the current slope, and the stored average), the memory required is 1 Gbyte.

The average photocurrent for every pixel is calculated at each OPD step by the instrument processor and then transferred to the spacecraft computer/memory systems. The data storage rate is 67 Mpixels/800 s $\times$ 2 FPAs $\times$ 2 byte = 330 Kbyte $s^{-1}$. With no data compression and/or data extension for error encoding, over the course of a day, this requires an on-board storage of 29 Gbytes and requires a transmission time of 6.4 hrs, assuming a rate of 10 Mbits $s^{-1}$. The IFIRS data storage requirement is a factor of 2.5 larger than previously discussed (Stockman et al. 1997); this is due to the larger number of pixels and shorter exposure time of the IFIRS system as compared to the ISIM yardstick.

In the mid-IR case, the integration time per OPD step is about 100 s. The data rate is now 4.2 Mpixels/100 s $\times$ 2 FPA $\times$ 2 bytes = 168 Kbytes $s^{-1}$, a slower overall rate than the near-IR. An even lower rate is possible if frames are coadded at each OPD step, to minimize the overhead associated with mirror movement.

Every interferogram measured with a four-port Michelson interferometer is a differential measurement between spectra of sources at the primary input and the spectra of the calibrator at the secondary input. Astronomical observations are always made with respect to the calibrator which acts as a transfer standard between measurements of astronomical standard stars. This intrinsic aspect of IFIRS is invaluable to the mitigation of systematic problems should FPAs, optical components, or enclosure temperature, suffer changes in characteristics due to long term exposure to the space environment.

## 3.3 Technology Readiness

### 3.3.1 Space Borne Fourier Transform Spectrometers

Fourier transform spectrometers have come to dominate laboratory IR spectrometry, remote sensing, and in space where broadband, high-resolution, precision radiometry is necessary. The IFTS is the logical evolution of the FTS, and is rapidly being adopted for satellite astronomy and remote sensing. The technology readiness of IFIRS can be assessed from the spaceflight heritage and performance of FTS systems on previous missions (e.g., Hanel et al. 1992; Beer 1992; Persky 1995) and the development and demonstration of IFTS systems by members of the IFIRS team (Bennett et al. 1993, 1994, 1995a, 1995b; Carter et al. 1994; Bennett 1997; Wurtz et al. 1999).

The capability of the FTS for serendipitous discoveries is best illustrated by the FTS instruments developed for planetary astronomy. Successfully demonstrated on Earth-observing missions (NIMBUS III and IV), the Infrared Interferometer Spectrometer (IRIS) instruments were the first of the long-duration, continuously operating space FTS systems (Hanel et al 1969, 1970, 1971, 1972a). Subsequent missions to Mars (Mariner 9, Hanel et al. 1972bc), and Jupiter, Saturn, Uranus, and Neptune (Voyager I, Hanel et al. 1979, 1980 and Voyager II,

Hanel et al. 1986, 1989; Courtin et al. 1984; Coustenis, 1989) redefined our understanding of the surface and atmospheric composition of the planets and their satellites. Voyager's discovery of Titan's chemically complex atmosphere was totally unexpected and motivated the Composite Infrared Spectrometer (CIRS) an imaging FTS on CASSINI (launched in 1997) to characterize the surface and atmosphere of Titan (Maymon et al. 1993; Kunde et al. 1996). The Thermal Emission Spectrometer (TES/M) on the Mars Global Surveyor (1998) has provided excellent surface maps throughout the mission lifetime (Christensen et al. 1992). On each of the planetary missions the FTS systems continued to operate until shutdown at the end of missions.

The FTS has been a key technique for measurements of the cosmic microwave background (CMB) from space (e.g., Gush, Halpern, & Wishnow 1990). The Far InfraRed Absolute Spectrophotometer (FIRAS) on the Cosmic Background Explorer compared the CMB radiation to an accurate blackbody and observed the spatial distribution of dust and Galactic line emission (Mather et al. 1993, 1994). For mid-infrared astronomy, the Spatial Infrared Imaging Telescope (SPIRIT III) sensor, developed for the Midcourse Space Experiment (MSX - 1996-99) by the Ballistic Missile Defense Organization demonstrated an FTS system for $2 - 28$ $\mu$m astronomical spectroscopy (Mill 1994; Zachor et al. 1994; Ames & Burt 1994; Burdick & Morris 1997). In 1998, ESA selected the Spectral and Photometric Imaging Receiver (SPIRE) which includes an IFTS for FIRST (Griffin 1998) and Japan is developing the Far-infrared Surveyor (FIS), also containing an IFTS, for the IR Imaging Surveyor (IRIS) satellite (Kawada 1998).

FTS instruments are the mainstay of IR sensors for meteorological and climate research (Shimoda & Ogawa 1994; de Zoeten et al. 1993; Endermann et al. 1994; Beer & Glavitch 1989; Javelle et al. 1994; Farmer 1987; Farmer et al. 1987; Farmer & Norton 1989ab; Farmer 1994; Abrams et al. 1996). One example has directly influenced the IFIRS design: the ATMOS interferometer, which flew on the Space Shuttle four times, did not require realignment between fabrication in 1982 and decommissioning in 1999 due to its optical configuration. "Aligned-by-design" optical systems, such as ATMOS, relax alignment tolerances and stability from arc-seconds to arc-minutes rendering the instrument insensitive to mechanical or thermally-induced misalignment (Farmer 1987).

### 3.3.2 Imaging Fourier Transform Spectrometers

Work by our partners at Bomem and at LLNL, has been directed towards technology demonstrations specific to an IFTS for NGST. The knowledge and experience accrued has guided our point design.

A group, co-founded in 1993 by Dr. C. Bennett at LLNL, has built several mid-IR IFTS systems, e.g., an IFTS equipped with $128 \times 128$ Si:As FPAs (Bennett 1995b), and operated them in adverse environments such as jet aircraft. Among the topics investigated with LLNL's IFTS mid-IR imagers are systems design, data acquisition, data reduction, image jitter, and source composition identification (Bennett et al. 1993; Carter et al. 1993a; Carter et al. 1995; Bennett et al. 1995ab; Bennett 1997).

LLNL has awarded R&D funds to Dr. K. Cook to develop a ground-based IFTS for astronomy and as a test-bed for NGST needs. The LLNL group has built a visible light, four-port IFTS for ground-based astronomical imaging (Fig. 13). Several technological and scientific demonstrations have been completed or are underway using this system. The visible is more challenging than the mid-IR because the wavelengths are much shorter. These observations

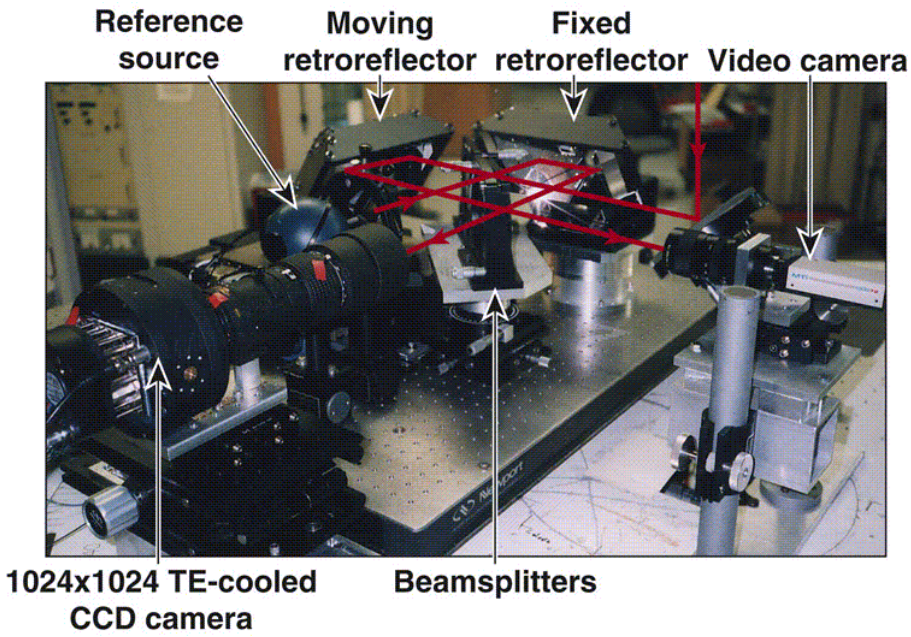


Figure 13: LLNL has designed, built, and run an visible light IFTS for low background astronomical use as a testbed for IFIRS. It is a four-port Michelson interferometer with self-compensating beamplitters and cube-corner retro-reflectors. The laser metrology system is attached to the moving mirror's motion stage, but below the science interferometer beam. This system was used at the 1.5-m McMath-Pierce Solar Observatory in March 1999 (Wurtz 1999). The science camera is an off-the-shelf CCD camera with a $1024 \times 1024$ thinned SITe chip thermoelectrically cooled to 235 K. The plate scale is $0.''4$ pixel$^{-1}$ with an unvignetted field of $5'$.

have low backgrounds and the exposure times are similar to those required by NGST. The short step sizes and long hold times provide a good testbed for NGST metrology. This instrument was fielded at the McMath-Pierce Telescope at Kitt Peak National Observatory and used to obtain color-magnitude diagrams for the globular cluster M 4 and data cubes of line emission from the Orion H II region (Wurtz et al. 1999). This interferometer has also made observations with small telescopes on-site at LLNL. Prisms have been used to obtain dispersed IFTS datasets to demonstrate source noise reduction. Two-output-port data have been used to demonstrate common mode noise rejection. The instrument is being modified for operation at the Lick 3-m and the Apache Point 3.5-m telescopes.

The Canadian Space Agency have awarded three contracts to our Canadian partners Dr. A. Villemaire (BOMEM) and Dr. S. Morris (Herzberg Institute of Astrophysics) to study an NGST IFTS. BOMEM has evaluated the trade space of an NGST instrument leading to an optimal IFTS design. An important focus of this effort has been to mitigate the risk associated with step scan operation. The challenge of maintaining the OPD stable for $1-10^3$ s is being evaluated with a prototype. Actuators are being tested in this demonstration as well as position servo controllers. The modularity of the prototype will give BOMEM the opportunity to evaluate different configurations and validate the results of the trade studies.

## 3.4 Technology Development

The items which require attention are listed in order of priority:

### 3.4.1 Focal Plane Arrays

Although progress has been substantial, the NGST detector goals have not yet been reached. In this regard IFIRS in full bandwidth mode is very tolerant of detector noise simply by virtue of the fact all the flux is focussed onto the detector, regardless of whether camera mode ($R \simeq 5$) or spectrally resolved data ($R \simeq 100$) is being acquired. IFIRS can use current state-of-the-art FPAs and obtain data with only minimal reduction of $SNR$ as compared to future FPAs with NGST requirements. It is the only proposed instrument capable of doing this. In dispersed mode IFIRS will require the proposed NGST low-noise FPAs to acquire the highest $SNR$ data.

IFIRS requires FPA developments which lead to large format focal plane systems. For the near-IR, $4096 \times 4096$ formats should be pursued to form the $8192 \times 8192$ system out of only four FPAs. Operation at 0.6 $\mu$m can be achieved with either InSb or HgCdTe, but at present, InSb has superior dark current performance compared to 5 $\mu$m cutoff HgCdTe (Vural 1998; Hoffman et al. 1998; Bailey et al. 1999). For the mid-IR, Si:As FPAs of $2048 \times 2048$ formats with current noise performance (Estrada et al. 1998), and well depths to accommodate flux over the full $5 - 28$ $\mu$m band are required. NGST specifications are for well depths of 60,000 $e^-$, whereas IFIRS requires well depths of a few million $e^-$ more characteristic of high background arrays used for ground-based astronomy (McCreight 1999). Si:As FPAs currently have low dark current levels which are far below the flux levels of scattered radiation from the sun-shield.

Two alternative mid-IR detector technologies are of interest. Si:Ga FPAs will ease requirements for cryocoolers to about 15 K because the band gap corresponds to a wavelength of about 17 $\mu$m. At present these arrays have a QE which is less than Si:As by about a factor of two (Hogue 1999). Long wavelength HgCdTe can operate near 30 K, eliminating cryocoolers. HgCdTe requires developments on two fronts: lower dark current and low power readout circuits. For 15 $\mu$m cutoff material the dark current should be comparable to the scattered light from the sun-shield, or about 1000 $e^-$ $s^{-1}$ $pix^{-1}$. The published capabilities of 16 $\mu$m cutoff material with 40 $\mu$m pixels is about $1 \times 10^8$ $e^-$ $s^{-1}$ at 40 K and can be extrapolated to $1 \times 10^7$ $e^-$ $s^{-1}$ at 30 K (Kozlowski et al. 1998). For 10 $\mu$m material, however, the dark current has been measured at about 300 $e^-$ $s^{-1}$ for single pixel detectors (Bailey et al. 1998). The Rockwell Science Center is working on improving dark current performance by reducing defects in the material and by using lower doping concentrations. There is a further difficulty with HgCdTe in that the bias applied to these small bandgap materials must be low, and to obtain a reasonable charge integrating capacity the multiplexer unit cell must be continuously powered. For NGST this involves developing low power multiplexer circuits. There is a reasonable expectation that substantial progress is possible with HgCdTe FPAs, and NGST should continue to support development efforts.

### 3.4.2 Beam-Splitters

The most crucial optical elements in IFIRS are the beam-splitters. The AR and 50:50 reflection/transmission coated surfaces must be of high quality (homogeneity and surface quality) over extended wavelength ranges and compatible with cooling to 25 K. The substrate materials most suitable for the mid-IR range tend to be relatively fragile. Although the wavefront quality requirement on the beam splitters is not much higher than for the remainder of the optical surfaces, the lack of choice in substrate materials and the lack of knowledge of their cryogenic performance is significant. The technology of broad-band, large, cryogenic beam-splitters must be developed.

### 3.4.3 Thermal and Mechanical Stability

Stable thermal-optical-mechanical designs for IFIRS exist as concepts. Concepts use aluminum alloy or composite materials, but ISIM choices affect IFIRS. Design strategies are: 1) make IFIRS intrinsically stable, i.e., athermalized; 2) make IFIRS changes track the ISIM; or 3) add active compensation to IFIRS. All concepts strive for minimum total variation and most include means for post-launch adjustment. Trade studies are needed to decide which of these is most compatible with NGST as a whole; ITT has the technology necessary to quantify these comparisons. ITT designers are familiar with tools to model the IFIRS optical system, mechanical structure, and thermal characteristics with acceptable accuracy and precision. Validated data sets describe the physical properties of the candidate materials, and the manufacturing processes are known.

Low temperature physics and experience teaches that cooling from 300 K to 30 K makes most optical materials more transmissive with a small decrease in index of refraction. Since there are no powered refractive elements in IFIRS, small uncertainties in the low temperature refractive indices of materials will not require a program to make new measurements under cryogenic conditions. The symmetry properties of a four-port Michelson interferometer cancels many effects, leaving an easily corrected phase offset. Coating choices for cryogenic optics are known, with known issues involving the coefficient of thermal expansion, thin film stress, process control, measurement, and uniformity. All are workable using design tools such as ASAP, CODE-V, and ITT-proprietary software for tolerancing; none are show-stoppers.

### 3.4.4 Laser Metrology

The wavelength stability and operability requirements of the metrology laser, operating in the NGST cryogenic environment, for a 5 year mission lifetime are demanding. Three classes of sources have been investigated: HeNe laser, neon lamp, and laser diode. Flight qualifying a HeNe laser for a long duration mission is a problem because He gas leaks from the plasma tube. Ne lamps lack brightness when operated for long life or lack life when operated at high brightness. Laser diodes offer excellent promise. Space qualification is practical and has been done for some missions, but not long lifetime missions (ITT's primary interest). The primary defect is wavelength stability, which depends on diode temperature, drive current, and operating time. ITT/Bomem have a patent (Optical Frequency Stability Controller, 5 757 488) that uses these dependencies to stabilize, long term with $<2$ PPM error, which is more than adequate for IFIRS.

ITT/Bomem have examined many classes of laser diodes for space flight use, and have chosen a distributed feedback (DFB) diode because it is highly resistant to mode hopping. DFB diodes are sensitive to optical feedback, a property that becomes important when using them with optical fibers. Commercial AlGaAs DFB diodes exist for 760—945 nm. ITT has an operating interferometer that uses an 852 nm diode in the metrology system and has flight qualification underway for this diode. Important attributes are life, vibration susceptibility, reliability, and radiation effects.

### 3.4.5 Programmable Focal Plane Masks

The ISIM studies led by Moseley and MacKenty are vigorously exploring micro-electro-mechanical systems (MEMS) technology to implement micro-shutter and micro mirror arrays. We have assumed in our point design that these programmable arrays are employed as a focal plane mask to adaptively select regions in the object plane for feeding to the dispersed mode of IFIRS. In the dispersed mode, it is the interferometer, not the prism, which determines the spectral resolution. Thus, compared to a pure dispersive spectrometer, only a relatively coarse slot ($1''$) is necessary. Although such arrays would add greatly to the efficiency of IFIRS for high spectral resolution observations, it would be possible to employ a non-programmable suite of slit masks for many of the needs of the dispersed FTS mode.

### 3.4.6 Optical Surface Quality

The wavefront quality requirements for the large cryogenic optics of the IFIRS point design are demanding, but no more so than for any other wide-field NGST imager. Diamond machined Al alloy optics for cryogenic TMAs routinely achieve 30 nm rms WFE (including mirror fabrication and profile errors) per surface (Robichaud et al. 1998). In the case of the NIRSPEC TMA, the largest single contribution to the fabrication error budget is due to the bi-metallic bending of the Al mirror substrate by the Ni coating during cryogenic operation. The Ni coating is used to facilitate optical polishing. In the near future it can be expected that the surface roughness of bare Al alloy without a post-polished coating will probably be satisfactory, if the corresponding 8% total system loss of throughput due to the reduced reflectivity of Al is acceptable (Vukobratovich et al. 1998).

### 3.4.7 Cryogenic Actuators

Cryogenic actuators are crucial to the success of NGST as they needed to actively adapt the surface figure of the OTA primary. NASA is heavily investing in this technology and is supporting seven external studies. IFIRS requires an actuator for controlling the interferometer OPD having a precision of approximately 1 nm, with a stroke of 10 mm.

These specifications are very comparable to those of the NGST goals (<10 nm resolution, >10 mm stroke) where the telescope system will require hundreds of these actuators. Once these systems are sucessfully demonstrated, for example the Inchworm II (Henderson & Fasick 1999), they can be incorporated directly into the IFIRS design. To mitigate risk, the original IFIRS design located this actuator in a 300 K environment, but discussions with the NGST team at GSFC has led us to adopt the cryogenic mechanism at 25 K.

| | Task Name | Duration | Start | Finish |
|---|---|---|---|---|
| 1 | Phase A Start | 0d | Sun 4/1/01 | Sun 4/1/01 |
| 2 | Syst. Reqmts. Review | 0d | Mon 6/4/01 | Mon 6/4/01 |
| 3 | FPA Technology Evaluation | 0d | Mon 6/4/01 | Mon 6/4/01 |
| 4 | Design/Analysis Activity | 263d | Mon 6/4/01 | Wed 6/5/02 |
| 5 | Syst. Functional Review | 0d | Mon 9/3/01 | Mon 9/3/01 |
| 6 | Prelim. Des. Review | 0d | Wed 6/5/02 | Wed 6/5/02 |
| 7 | Long Lead Procurements | 430d | Thu 6/6/02 | Wed 1/28/04 |
| 8 | Critical Design Review | 0d | Mon 6/2/03 | Mon 6/2/03 |
| 9 | Short Lead Procurements | 150d | Tue 6/3/03 | Mon 12/29/03 |
| 10 | Assembly | 125d | Mon 2/2/04 | Fri 7/23/04 |
| 11 | Integration | 120d | Mon 7/26/04 | Fri 1/7/05 |
| 12 | Final Test | 100d | Mon 1/10/05 | Fri 5/27/05 |
| 13 | Ship Inst. to NASA/GSFC | 0d | Thu 6/2/05 | Thu 6/2/05 |
| 14 | Int. & Test, Field Support | 650d | Mon 6/6/05 | Fri 11/30/07 |

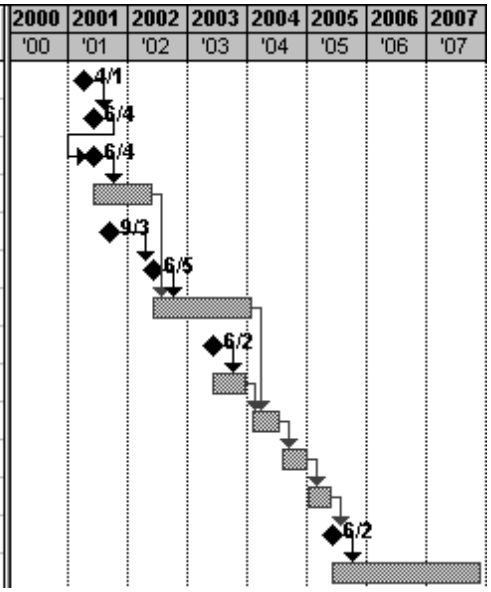


Figure 14: Top level NGST/IFIRS schedule

## 3.5 Schedule

### 3.5.1 Development Schedule

The initial activities of the Development Phase will focus upon: 1) team structuring; 2) interfacing with NASA/GSFC personnel regarding the OTA optical prescription and the ISIM architecture, design parameters and constraints; 3) preliminary interfacing with the FPA manufacturer. These activities will permit the team to establish a preliminary set of system requirements and an update of the conceptual design discussed in section 3.2. A formal Systems Requirements Review is scheduled for June 2001.

The availability of the FPA technology menu in June 2001 will permit starting preliminary designs and conceptual design options. Paramount data required include detector pitch, format size, and tiled (mosaiced) packing density. Performance modeling will need data for dark current, read noise and charge capacity.

The next major milestone is a Systems Functional Review in September 2001 as shown in Fig. 14. During this three month period, technical interfacing will occur with prospective suppliers in the areas of 1) optics, particularly mirrors and beam-splitter substrates; 2) structures; 3) cryogenic actuators; and 4) signal processors.

During this same period, June-August 2001, the preliminary optical design will mature thereby permitting optical sensitivity analysis to proceed. At this point an integrated thermal-structural-optical analysis can be initiated for one or more candidate materials in support of the trade studies identified above. These analyses would then be transferred to NASA/GSFC for inclusion into an integrated ISIM thermal-structural-optical analysis. This will spawn a detailed system level dialog assuring reduced risk.

### 3.5.2 Integration and Test Plan

IFIRS is conceived as protoflight hardware built from tested, flight-qualified sub-assemblies and modules. Systems engineers will define the IFIRS functional architecture and the mapping of function onto physical hardware and software modules. Trade studies and experience will guide this process. The goal is an instrument which is formed from testable subsystems and modules that easily assemble as a stable and aligned instrument.

Integration plans will begin with the hardware and software modules of IFIRS. Hardware modules, built from designs qualified by engineering tests, will be subjected to flight model acceptance tests which combine environmental stress and performance evaluation. Stress testing will reveal faulty workmanship. Performance testing will confirm that each module meets all of its functional requirements. Testing of IFIRS modules will include cycling from room temperature to cryogenic operating temperature plus performance tests at operating temperature. For IFIRS optical-mechanical modules this means testing at 30 K using NASA (ARC or MSFC), CSA (David Florida Lab), or commercial facilities. The IFIRS detectors will be tested at operating temperature at the supplier.

Flight software, assembled from modules qualified by development test, will be the subject of preliminary acceptance tests in an engineering model subset of IFIRS. There are two major software configuration items: real-time code embedded in the IFIRS hardware and signal processing code executed in a NASA-supplied processor in the ISIM.

ITT will combine IFIRS hardware and software modules into the IFIRS instrument, and align and test the IFIRS at room temperature using special optical test equipment and data acquisition electronics. The data acquisition equipment will be able to simulate the ISIM-located processor. This testing will confirm that the IFIRS instrument functions at room temperature, communicates with the planned signal processor, and executes a test suite of signal processing functions.

Integration of IFIRS hardware with the ISIM and software with the ISIM-located signal processor will take place at a NASA facility, as will vibration and low temperature testing. The engineering and test teams will support these NASA activities with IFIRS-specific equipment, plans and procedures. Operation and performance testing at the cryogenic operating temperature (e.g., 30 K) is desirable but expensive. Higher temperature tests can be accommodated if known at design-time. For example, detector sub-assemblies can include dewar enclosures that allow the FPA to operate at 30 K or less while the rest of the IFIRS and ISIM operate at $LN_2$ temperature.

Throughout all integration and test activities, ITT will collect engineering and performance data for comparison with values expected from design and simulation activities. Deviations will prompt investigation of the cause and determination of prudent corrective action. The IFIRS team will also use this data to monitor trends in the instrument's characteristics. Trends give confidence that the IFIRS continues to perform as designed, that it remains healthy with full capability to produce high quality scientific data.

The IFIRS team support will continue throughout the NGST life cycle, including pre-launch, post launch, and mission operations.

Table 3: **IFIRS Cost Summary[a] (Real Year US Dollars (K))**

| WBS Element | Phase A | Phase C | Total (A+C) | GFE[b] Fraction of Total (%) | Total Cost Including GFE |
|---|---|---|---|---|---|
| 1.0 Management | 4,478 | 4,629 | 9,107 | 0 | 9,107 |
| 2.0 Science Program | 4,218 | 10,325 | 14,543 | 0 | 14,543 |
| 3.0 Systems Engineering | 11,376 | 4,478 | 15,854 | 17 | 19,101 |
| 4.0 SR and QA | 2,266 | 3 | 2,269 | 0 | 2,269 |
| 5.0 Structure | 17,995 | 5,616 | 23,611 | 31 | 34,219 |
| 6.0 Optics | 31,016 | 7,229 | 38,245 | 0 | 38,245 |
| 7.0 Electronics | 4,862 | 653 | 5,515 | 20 | 6,894 |
| 8.0 Thermal Engineering | 2,018 | 0,000 | 2,018 | 10 | 2,242 |
| 9.0 Software | 3,746 | 0,000 | 3,745 | 0 | 3,745 |
| 10.0 Detectors | 0,000 | 0,000 | 0,000 | 100 | 75,000 |
| Program Totals | 81,975 | 32,932 | 114,909 | 44 | 205,365 |

[a] The Rough Order of Magnitude estimates included herein are presented for budgetary planning purposes only and should not be construed as a firm offer. ITT will be pleased to prepare a firm proposal upon NASA's request when requirements for the program are better defined.
[b] The GSFC WBS calls out Elements 3, 5, 7, 8, &, 10 as partially Government furnished equipment (GFE). This column reflects *our* estimate of the cost of these items.

# 4 COST ESTIMATE

## 4.1 Cost Summary

This section provides Level 1 and Level 2 cost details for the ROM cost estimate requested in the SOW, paragraph 2(i). We have used the WBS organization requested in the Final Report Format, note 6. The costs are delineated by phase: instrument Phase A beginning in April 2001 and Phase C beginning in June (assumed) 2003.

The IFIRS configuration costs presented below include aluminum alloy optics, auxiliary structures, the necessary electronics boxes to be operated at 220 K, the detector front-end off-chip electronics, transit cases, Integration and Test labor, support at GSFC for observatory level integration, and pre-launch science support. Costs for GFE provided ISIM services, including: supporting structure, instrument optical bench cooling, detector front end electronics package and FPA's, and the flight data system and instrument control processor have been estimated, but are presented separately in the GFE column.

Phase A costs include material costs for the IFIRS flight hardware. If this procurement is deferred until Phase C, the Phase A cost is reduced by approximately $14M, and the Phase C cost increases accordingly.

## 4.2 Cost Details

This section provides additional detail on the above IFIRS cost estimate, with details down to Level 3. Cost estimate assumptions are provided in Section 4.2.1, including a discussion

of items that are assumed to be GFE. The costing methodology is described in Section 4.2.2. A preliminary WBS dictionary is provided in Section 4.2.3. A breakout of Level 3 costing data is included in Section 4.2.5. De-scope options with associated Level 1 cost estimates are provided in Section 4.2.6.

### 4.2.1 Instrument Configuration Assumptions

The cost estimate corresponds to a dual-band dual-focal plane assemblies instrument with a mode switchable set of beam-splitters and beam combiners. The respective fields of view are $5.'28 \times 5.'28$ for the near-IR band and $2.'64 \times 2.'64$ for the MIR band.

The cost estimate assumes the following items to be government furnished: 1) FPAs and on-chip readout electronics, 2) high level signal processors, 3) computer based processors for decimating, packetizing and telemetering of the data, and 4) a monocoque optical bench configured to accept the f/15 to f/24 re-imaging relay optics, the IFIRS instrument, and any other instruments selected by the government, and internally interfaced to the ISIM structure.

An environmentally based transit case with appropriate mechanical attributes and low-boy transporter for over-the-road or air lifting are included in our estimate.

### 4.2.2 Costing Methodology

Two primary costing tools were used to develop our IFIRS cost estimates: the SEER-H parametric cost model, and a set of historical metrics based on prior ITT space hardware development programs.

For WBS items 5.0 and 6.0 (Structure and Optics), the parametric cost modeling tool referred to as SEER-H was employed. This modeling tool has been validated against prior ITT space hardware programs. For example, the SEER model was employed under an IR&D program for calibration for evaluating the GOES object plane pocketed scan mirror when constructed from aluminum alloy, beryllium, carbon/silicon carbide composite and reaction bonded optical grade SiC. The model cost compared favorably (5%) with vendor actual cost.

For the remaining WBS elements, a standardized set of ITT metrics for the design and manufacture of space payloads were used. These metrics were developed from prior experience on other space programs. The metrics utilize input factors such as number and complexity of electronics circuit cards or mechanical assemblies, lines of software code, number of specifications, and other similar parameters. These metrics have been validated against actual costs on recent space programs. Where appropriate, material costs from similar space hardware components have also been used as the basis for material cost estimates.

Estimates for WBS 2.0 were augmented by inputs from LLNL and UC Berkeley. These estimates are based on prior experience on similar space science programs. Imported costs also considered consultants and travel elements.

### 4.2.3 WBS Dictionary

**1) Management** This element includes all efforts required to provide program management. It includes planning, technical direction, schedules, budgets, earned value, documentation, and control of all program efforts including program management functions for the major subcontractors. Travel and consultant fees are included.

**2) Science Program Development** This element includes all efforts associated with the academic partners, team astronomers and associated government agencies contributing to the science program development. Resources for on site support for ISIM integration at GSFC, pre-launch support for the guaranteed time observing program, and observatory level integration are included.

**3) Systems Engineering** This element includes the effort required to generate the overall IFIRS instrument requirements, which include the instrument and its test equipment. It includes definition of system requirements and interfaces so that the individual subsystem designs may advance in a unified manner. The systems engineering WBS element also includes integration, test and evaluation activities for the IFIRS instrument. This will be a continuing effort starting with system definition and following through to final performance tests and calibration.

**4) SR&QA** This element includes all of the efforts related to the NGST/IFIRS reliability and quality assurance program. This includes planning and implementation of all efforts in the areas of reliability, quality assurance, system safety and parts programs.

**5) Structure** This element includes generation and maintenance of all structural analyses necessary to assure that the instrument will satisfy the specifications. Close technical interfacing with (1) NASA GSFC regarding the main optical bench within the ISIM structure, (2) the optical design and tolerancing activity, and (3) the thermal analyses and thermal management activities are included. See also WBS Element 8. Also included are the procurement, integration and test activities associated with the structural components and all mechanisms.

**6) Optics** This element includes development of an optimized optical prescription, sensitivity tables, tolerance studies, opto-mechanical error budgeting and performance predictions for the IFIRS relay optics and the interferometer optics. Also included are the procurement, integration and test activities associated with the optical components and modules. It is expected that the major components with power will be fabricated and cryo null figured at a suitable vendor and cryo tested at an appropriate facility such as NASA ARC or NASA MSFC.

**7) Electronics** This element includes generation and maintenance of all electrical/electronic analyses necessary to assure the IFIRS instrument will satisfy the specifications. These activities specifically consider the interfacing to GFE'd FPA on-chip electronics, intermediate signal processing electronics, interfacing to the GFE'd signal processing computer, the servo control loop and the metrology laser within the interferometer module, and control of all dynamic mechanisms and actuators. Also included are the procurement, integration and test activities associated with the electronics.

**8) Thermal** This element includes generation and maintenance of all thermal analyses necessary to assure that the IFIRS instrument will satisfy the specifications and specifically yield an athermalized design. Close technical interfacing with NASA GSFC regarding the main optical bench within the ISIM structure, the optical design and tolerancing activity, and structural mechanical engineering are included. Together with elements 5 and 6 an integrated thermal-structural-optical model will be developed for internal peer review and direct interfacing with NASA GSFC personnel. This integrated model will rely heavily upon the NASTRAN mathematical model for linear/non- linear static and dynamic analyses of structures and the TRASYS and SINDA mathematical models for the thermal design and heat transfer analyses.

**9) Software** This element includes the generation and maintenance of all software routines required by the IFIRS instrument but does not include higher level observatory facility software to be developed by NASA GSFC. Specifically included are interferometer Flight control software (3,700 lines of code), data processing software (15,000 lines), and ground test software (16,300 lines).

**10) Detectors** This element includes all aspects for the procurement and integration of the focal plane assemblies. As these assemblies are GFE'd, this element serves as a placeholder.

### 4.2.4 Mass, Volume, & Power Estimates

A key element in the estimation of costs is the estimate of mass, volume, and power. The estimates for these quantities are listed in the Table 4. As with the costing exercise, the IFIRS mass estimates assume aluminum alloy optics and include estimates of GFE support structure. A majority of the IFIRS mass estimate is the optical bench which is logically a significant portion of the ISIM structure; the residual 523 kg mass estimate for IFIRS is relatively consistent with typical instrument:satellite ratios at 15%.

Table 4: **Mass, Volume, and Power**

| Segment | Component | Mass (kg) | Volume ($m^3$) | Power (W) |
|---|---|---|---|---|
| Optical Bench | | 800 | 14.6 | |
| Collimator | Optics | 39 | | |
| | Fold Mirror | 10 | | |
| | Flexures | 4 | | |
| | Truss | 28 | | |
| | | 81 | | |
| Interferometer | Carriage | 19 | | |
| | Fixed Retro. Support | 10 | | |
| | Moving Retro. Support | 10 | | |
| | Retroreflectors | 22 | | |
| | 1st Port Ent. Mirror | 2 | | |
| | 2nd Port Ent. Mirror | 2 | | |
| | Beamsplitters (2) | 15 | | |
| | Beamcombiners (2) | 15 | | |
| | Bearings | 5 | | |
| | | 100 | | |
| Camera Objectives (2) | Optics | 48 | | |
| | Flexures | 4 | | |
| | Truss | 75 | | |
| | Dichroic Filters (2) | 66 | | |
| | Filter Supports | 79 | | |
| | | 272 | | |
| Focal Plane Assemblies (2) | NIR FPAs | 2 | | 44 |
| | MIR FPAs | 1 | | 58 |
| | NIR FPA Supports | 29 | | |
| | MIR FPA Supports | 16 | | |
| | | 48 | | 102 |
| Processors | NIR | 16 | | 209 |
| | MIR | 6 | | 75 |
| | | 22 | | 284 |
| Totals | | 1323 | 14.6 | 386 |

Table 5: **Level 3 Cost**

| WBS | WBS Title | Material Cost ($M) | Total Cost ($M) |
|---|---|---|---|
| **1** | **Management** | **0.649*** | **9.107** |
| 1.1 | Program Management | 0 | 1.020 |
| 1.2 | Financial | 0 | 0.510 |
| 1.3 | Schedule/administrative | 0 | 1.020 |
| 1.4 | Contracts | 0 | 0.510 |
| 1.5 | Subcontracts | 0 | 2.041 |
| 1.6 | Data Management | 0 | 0.255 |
| 1.7 | Travel | 0.649* | 0.649 |
| 1.8 | Engineering Leadership | 0 | 2.081 |
| 1.9 | Operations Leadership | 0 | 1.020 |
| **2** | **Science Program Development** | **12.331**** | **14.543** |
| 2.1 | LLNL Science Support | 6.517** | 6.517 |
| 2.2 | Academic Science Support | 5.814** | 5.714 |
| 2.3 | ITT Science Support | 0 | 2.212 |
| **3** | **System Engr., Integr., Test (SEIT)** | **4.607** | **15.854** |
| 3.1 | Mission Analysis | 0 | 0.566 |
| 3.2 | Trade Studies | 0 | 0.860 |
| 3.3 | Concept Development | 0 | 1.173 |
| 3.4 | Specification Development | 0 | 0.809 |
| 3.5 | Spacecraft Interfaces | 0 | 0.598 |
| 3.6 | Risk Management / Risk Reduction Demos | 2.375 | 2.086 |
| 3.7 | Configuration Management | 0 | 0.067 |
| 3.8 | System Integration and Test | 2.232 | 7.898 |
| 3.9 | Post Delivery Support (Engineering) | 0 | 0.143 |
| 3.10 | Major Reviews | 0 | 1.354 |
| **4** | **SR & QA** | **0** | **2.269** |
| 4.1 | Quality Assurance | 0 | 0.899 |
| 4.2 | Reliability | 0 | 0.507 |
| 4.3 | Software QA | 0 | 0.788 |
| 4.4 | Vendor Liasons / Source Inspections | 0 | 0.074 |
| **5** | **Structure** | **2.253** | **23.611** |
| 5.1 | Optical Bench | 0.487 | 6.824 |
| 5.2 | Surrogate Collimator Bench | 0.146 | 2.602 |
| 5.3 | Entrance Mirror Support | 0.118 | 2.028 |
| 5.4 | Collimator Truss | 0.081 | 1.041 |
| 5.5 | Exit Mirror Support | 0.044 | 0.606 |
| 5.6 | Surrogate Camera Objective Bench | 0.227 | 2.815 |
| 5.7 | Camera Objective Truss | 0.104 | 1.685 |
| 5.8 | NIR Detector Supports | 0.035 | 0.476 |
| 5.9 | MIR Detector Supports | 0.022 | 0.295 |
| 5.10 | Dichroic Filter Supports | 0.084 | 1.149 |
| 5.11 | Beamsplitter Frame | 0.142 | 0.359 |
| 5.12 | Fixed Cube Mirror Support | 0 | 0.293 |
| 5.13 | Moving Cube Mirror Support | 0.533 | 1.768 |
| 5.14 | Carriage | 0.044 | 0.605 |
| 5.15 | Module Ass'y Fixturing | 0.082 | 0.395 |
| 5.16 | Transporter Facility | 0.081 | 0.562 |
| 5.17 | Low boy Dolly | 0.023 | 0.107 |

| WBS | WBS Title | Material Cost ($M) | Total Cost ($M) |
|---|---|---|---|
| **6** | **Optics** | **8.267** | **38.245** |
| 6.1 | Collimator | 0.093 | 4.943 |
| 6.2 | LUPI/Cryo Fixtures | 0.202 | 1.867 |
| 6.3 | Interferometer | 2.398 | 9.464 |
| 6.4 | Retroreflectors | 0.203 | 3.017 |
| 6.5 | Camera Objectives | 0.115 | 3.009 |
| 6.6 | Dichroics | 4.410 | 12.973 |
| 6.7 | Auto Alignment Telescopes | 0.023 | 0.093 |
| 6.8 | Zenger Prism Assembly | 0.825 | 2.878 |
| **7** | **Electronics** | **1.057** | **5.515** |
| 7.1 | IFIRS Control Electronics Design / Build | 0.089 | 0.702 |
| 7.2 | Interferometer Control Electronics Design / Build | 0.357 | 1.525 |
| 7.3 | NIR/MIR Signal Collection Electronics Design/Build | 0.406 | 1.163 |
| 7.4 | Parent Boards Design / Build | 0.045 | 0.838 |
| 7.5 | Power Supply Design / Build | 0.037 | 0.241 |
| 7.6 | Electronics Box Design / Build | 0.025 | 0.322 |
| 7.7 | Harness Design / Build | 0.097 | 0.724 |
| **8** | **Thermal Engineering** | **0** | **2.018** |
| **9** | **Software** | **0.009** | **3.745** |
| 9.1 | Flight Software - Embedded in IFIRS Hardware | 0 | 0.617 |
| 9.2 | Flight Software - Signal Processing in NASA Hardware | 0 | 2.364 |
| 9.3 | Test Software Development | 0.009 | 0.764 |
| **10** | **Detectors** | **0.00** | **0.000** |
| | | **Total Material ($M)** | **Total Cost ($M)** |
| | | **16.193** | **114.909** |

*The Rough Order of Magnitude estimates included herein are presented for budgetary planning purposes only and should not be construed as a firm offer. ITT will be pleased to prepare a firm proposal upon NASA's request when requirements for the program are better defined.*

* *Travel Costs are Included Under Travel (Not Materials) in Detailed Summary*

** *LLNL and Academic Science Support is included Under Subcontracts (Not Materials) in Detailed Summary*

### 4.2.5 Level 3 Cost Breakdown

A more detailed breakout of Level 3 costs is provided which includes labor hours and material costs for each sub-element of the WBS.

### 4.2.6 De-scope Options

The principal trades are cost vs. observing time and package size vs. observing time. If the second output port was eliminated the associated recurring FPA costs would be halved and the resulting recurring powered optics fabrication and alignment costs would be reduced by one-third. The drawbacks of this option are the increased integration time and the loss of immunity to temporal background variations. Furthermore, the redundancy in the event of a failure in one of the output streams, whether in the optics, the detectors, or the data handling chain, would be lost. The overall factor of two loss of speed, the greater susceptibility to systematic errors, and the loss of redundancy make this an undesirable de-scope.

De-scope options having the greatest impact on system cost and risk, while maintaining a large degree of scientific integrity, are: 1) decrease the field of view; 2) decrease the spectral coverage. With the first option, the principal trade is cost vs. field of view. Reducing the near-IR FPAs from $8192 \times 8192$ to $4096 \times 4096$ would yield a FOV of $2.'64 \times 2.'64$ unless the camera objectives effective focal length (EFL) were altered. In terms of cost the resulting FPAs would

be about one-fourth of the baseline cost. As the TMA collimator and TMA camera will be somewhat smaller, one might expect a 10-15% cost reduction for these elements.

IFIRS implemented with only a near-IR or mid-IR only is a very competent scientific instrument. The mid-IR only version of IFIRS is an economical instrument with unmatched discovery potential.

Should cryocoolers for the ISIM be rejected for reasons of cost, reliability, or power consumption, the mid-IR capability need not be abandoned. IFIRS in full band mode is tolerant of a large detector dark current. For example, a dark current of 1000 $e^-$ $s^{-1}$ $pix^{-1}$ yields about 1/3 of the total background signal including scattered sun-shield radiation and the zodiacal light over the 5-15 $\mu$m waveband. Should HgCdTe long wavelength detectors be developed with dark currents of this order, the reduction in $SNR$ is small as compared to Si:As detectors. Currently existing HgCdTe FPAs covering the band 5-10 $\mu$m might be usable to preserve a limited mid-IR capability were cryocoolers deemed infeasible. With further development it is hoped that this wavelength limit will be extended.

The following IFIRS de-scope options have been costed:

1. Near-IR & Mid-IR bands with a 2.′64 square field of view
2. Near-IR band only with a 2.′64 square field of view
3. Mid-IR band only with a 2.′64 square field of view
4. Mid-IR band only with a 1.′32 square field of view

Level 1 estimated costs derived from the details of the previous section are shown in Table 6.

Table 6: **De-Scope-Configuration Level 1 Estimated Costs**

| Option | Description | Estimated Cost (Real Year k$ US) |
|---|---|---|
| 0 | 5.′28 Near-IR & 2.′64 Mid-IR | 114,909 |
| 1 | 2.′64 Near-IR & Mid-IR | 79,721 |
| 2 | 2.′64 Near-IR | 75,418 |
| 3 | 2.′64 Mid-IR | 74,208 |
| 4 | 1.′32 Mid-IR | 65,231 |

## 4.3 Past Performance Heritage

ITT Industries, along with its associate supplier, BOMEM, Inc., has a unique combination of interferometer design experience and an extensive background in designing remote sensing instruments for operational satellite payloads. These are the POES and GOES series of visible/IR Imagers and Atmospheric Sounders (which fly in LEO and GEO orbits, respectively). Interferometer designs include the NPOESS Cross-track Infrared Sounder (CrIS), and the GOES High Resolution Interferometer Sounder (GHIS) ITT has all the required engineering tools to perform on this program including a mature Systems Engineering process, interferometer and IFTS modeling and simulation capability, scene modeling, performance sensitivity

modeling, image reconstruction capability, and detail design capability in all engineering disciplines required to produce an IFTS for NGST.

### 4.3.1 Past Performance

Spanning more than thirty years, ITT has extensive experience in the design, fabrication, testing, and on-orbit operation of remote sensing instruments for meteorological observations from research and operational satellites. ITT is the world leader in instrumentation for operational weather satellites: if you watched the weather report last night, most likely, the satellite imagery was obtained with an ITT instrument. The instruments continue to exceed design expectations; of the thirty instruments launched between 1978 and 1996, all have exceeded their projected lifetimes (typically 2 years) by several years, redefining on-orbit reliability and performance. The current NOAA requirement of a 5 year lifetime is a direct result of the on-orbit performance of ITT sensors. Such performance is a product of experience tempered with a commitment to development and integration of new technologies, which provide improved capabilities with manageable risk, as indicated by the seventeen additional instruments in storage or fabrication. Current electro-optical instrumentation programs are listed below.

ITT has been awarded the development and fabrication contract for the next generation of polar-orbiting weather sensors and will produce three Cross-Track Infrared Sounders (CrIS), with an option for a fourth unit, for launch into orbit. CrIS, is a FTS instrument for nadir sounding. The non-recurring investment in CrIS will provide significant leverage for an IFTS on NGST, with many common components and technologies.

### 4.3.2 Cost and Schedule Control

The ITT team systems engineering process is executed by an Integrated Product Team (IPT), which includes the customer. The IPT establishes a conceptual design, conducts trade studies, algorithm development, tool building activities, and studies necessary to reduce the risks to a level low enough to proceed to a detailed design after preliminary design review. The IPT is the decision-making body on the ITT program. The System Engineering Integration team (SEIT) is responsible for executing the ITT Team's system engineering process and consists of the Lead Systems Engineer, leads of other IPTs, a System Performance Simulation (SPS) Engineer and a System Test Engineer. This process is derived from the MIL-STD-499B. The ITT Integrated Product Development (IPD) process, including the systems engineering process is compliant to ISO 9001. Cost is controlled by including it as a variable in the trade studies.

### 4.3.3 Facilities

ITT has the necessary facilities for calibration, thermal vacuum chambers, vibration equipment, electromagnetic interference, and radiation testing to support instrument development, qualification, and performance validation. Additionally, a key feature of the sensor development is the use of an end-to-end modeling and simulation capability which permits concise cost benefit analysis of performance trade studies supported with calibrated instrument/interface models (mechanical, thermal, electrical, and cost).

Table 7: **Synopsis of government sponsored past performance heritage space programs conducted by ITT's Aerospace/Communications Division.**

| **Program Name** | NPOESS VIIRS and CrIS (Visible/IR Imager Radiometer Suite & Cross-track IR Sensor) | Polar Operational Environmental Satellite (POES) K-N' | GOES High Resolution Interferometric Spectrometer/Double Rate Imager (GHIS/DRI) | Geostationary Operational Environmental Satellite (GOES) N->Q | Geostationary Operational Environmental Satellite (GOES) I->M | NPOESS CrIS (Cross-track IR Sensor) |
|---|---|---|---|---|---|---|
| Contracting activity, address, telephone & fax number | Space & Missile Sys. Ctr. SMC/ CIKC Los Angeles AFB El Segundo, CA 90245 (310) 336-4335 Fax: (310) 336-4522 | NASA GSFC Greenbelt, MD 20771 (301) 286-7898 Fax: (301) 286-1699 | NASA GSFC Greenbelt, MD 20771 (301) 286-7898 Fax: (301) 286-1699 | NASA GSFC Greenbelt, MD 20771 (301) 286-7898 Fax: (301) 286-1699 | (Subcontract to Loral) NASA GSFC Greenbelt, MD 20771 (301) 286-7898 Fax: (301) 286-1699 | Space & Missile Sys. Ctr SMC/ CIKC Los Angeles AFB El Segundo, CA 90245 (310) 336-4335 Fax: (310) 336-4522 |
| Procuring Contracting Officer's name, telephone & fax number | Capt. Mario Troncoso (310) 336-4335 Fax: (310) 336-4522 | Mr. Steven Lloyd (301) 286-7898 Fax: (301) 286-9777 | Mr. Steven Lloyd (301) 286-7898 Fax: (301) 286-9777 | Ms. Clelia Walker (301) 286-1351 Fax: (301) 286-9777 | Ms. Clelia Walker (301) 286-1351 Fax: (301) 286-9777 | Capt. Mario Troncoso (310) 336-4335 Fax: (310) 336-4522 |
| Customer Technical Representative telephone & fax number | VIIRS: Capt. Berry CrIS: Don Blersch (301) 427-2077 Fax: (301) 427-2164 | Mr. Doug Fineberg (301) 286-9842 Fax: (303) 286-1699 | Mr. David Martin (301) 286-3232 Fax: (303) 286-1700 | Ms. Pam Sullivan (301) 286-3750 Fax: (301) 286-9777 | Ms. Pam Sullivan (301) 286-3750 Fax: (301) 286-9777 | CrIS: Don Blersch (301) 427-2077 Fax: (301) 427-2164 |
| Contract number | F04701-97-C-0029 | NAS5-30384 | NAS5-32981 | NAS5-96090 | NAS5029500 to SS/L (SC-922800-AZ) to ITT | |
| Contract type | CPFF | CPFF/AF | CPFF | CPIF/AF | CPFF/AF | CPFF/AF |
| Final projected price/cost | $35,740,180.00 | $96,462,668.00 | $9,014,024.00 | $110,802,205.00 | $321,824,621.00 | $73,000,000.00 |
| **Primary Objectives** | Develop next generation LEO Imager & Sounder Radiometric Instruments | Delivery of 7 suites,i.e. Deliver 14 radiometers: 7-- AVHRR & 7-- HIRS | Develop next generation GEO Imager & Sounder Radiometers | Delivery of 4 Suites, i.e. Deliver 8 radiometers: 4-- Imagers & 4-- Sounders | Develop current generation of GEO Imagers & Sounders & Delivery of 5 Suites, i.e. Deliver 10 radiometers | Development of next generation LEO Sounder Radiometric Instruments/ Delivery of 3 FTS radiometers |

### 4.3.4 Conclusions

For both the study and implementation phases of new systems development, ITT can readily provide the multi-functional support required to bring a concept into operational use. Our competence in successful systems development and evolutionary advancements of both LEO and GEO remote sensor payloads is summarized in the foregoing overviews. It can be surmised from this brief documentation of experience that we are fully qualified and retain all the capabilities to meet the requirements required for proper execution of the program.

A synopsis of government sponsored past performance heritage space programs conducted by ITT's Aerospace/Communications Division is shown in Table 7.

# 5 References


Abrams, M. C., et al. 1996, Remote sensing of the Earth's atmosphere from space with high-resolution Fourier-transform spectroscopy: development and methodology of data processing for the Atmospheric Trace Molecule Spectroscopy experiment, Appl. Opt.,35, 2776

Ames, H. O.; Burt, D. A. 1994, Development of the SPIRIT III Sensor, Proc. SPIE 2227, 74-86

Bailey, R. et al., 1998, Proc. SPIE, 3354, 77

Beer, R. 1992, Remote Sensing by Fourier Transform Spectrometry , John Wiley and Sons, New York, N. Y.

Beer, R., & Glavitch, T. A. 1989, Remote sensing of the troposphere by infrared emission spectroscopy; Advanced Optical Instrumentation for Remote Sensing of the Earth's Surface from Space, Proc. SPIE, 1129, 42

Bennett, C. L., Carter, M. R., Fields, D. J., Hernandez, J. A. 1993, Imaging Fourier transform spectrometer, Proc. SPIE, 1937, 191

Bennett, C. L. 1997, Effect of jitter on an imaging FTIR spectrometer, Proc. SPIE, 3063, 174-184

Bennett, C. L. 1994, Fourier transform IR measurements of thermal infrared sky radiance and Transmission, Proc. SPIE, 2266, 25-35

Bennett, C. L., Carter, M. R., Fields, D. J., Lee, F. D. 1995a, Infrared hyperspectral imaging results from vapor plume experiments, Proc. SPIE, 2480, 435

Bennett, C. L., Carter, M. R., Fields, D. J. 1995b, Hyperspectral imaging in the infrared using LIFTIRS, Proc. SPIE, 2552, 274-283

Bennett, C. L. 2000, in Imaging the Universe in Three Dimensions: Astrophysics with Advanced Multi-Wavelength Imaging Devices. ASP Conference Series, W. van Breugel & J. Bland-Hawthorn (eds.), astro-ph/9908245

Bershady, M., et al., 1998, ApJ, 505, 50

Burdick, S. V.; Morris, D. C. 1997, SPIRIT III calibration stars: inband irradiance and uncertainty, Optical Engineering 36(11), 2971

Carlberg, R. G. et al., 1999, ApJ, In Preparation.

Carr, J.S., and Najita, J. 1998, in "Science with the NGST" eds., E.P. Smith and A. Koratkar, ASP Conf. Ser., vol. 133, p. 163

Carter, M. R.; Bennett, C. L.; Fields, D. J.; ; Hernandez, J. A., Gaseous effluent monitoring and identification using an imaging Fourier transform spectrometer 1994, Proc. SPIE, 2092, 16

Carter, M et al., 1995. Proc. SPIE 2480, 380

Christensen, P. R., et al., 1992, J. Geophys. Res., 97, 7719

Conrath, B. J., et al., Infrared observations of the Neptunian system , 1989, Science, 246, 1454

Courtin, R., et al., The composition of Saturn's atmosphere at northern temperate latitudes from Voyaer IRIS spectra: $NH_3$, $PH_3$, $C_2H_2$, $C_2H_4$, $CH_3D$, $CH_4$, and the Saturian D/H isotopic ratio , 1984, Astrophysical Journal, 287, 899

Coustenis, A., et al., Titan's atmosphere from Voyager infrared observations I. The gas composition of Titan's equatorial region , 1989, Icarus, 80, 54

Dahlen, T. and Fransson, C. 1998, in The Next Generation Space Telescope: Science Drivers and Technological Challenges , 34th Liege Astrophysics Colloquium, 237

Dey, A., Spinrad, H., Stern, D., Graham, J.R., Chaffee, F. 1998 ApJ, 498, L93

Dickinson, M. 1999, in After the Dark Ages: When Galaxies were Young , eds. S. Holt and E. Smith, American Institute of Physics Press, p. 122

Endermann, M., Lange, G., and Fladt, B., Michelson Interferometer for Passive Atmospheric Sounding; Space Optics 1994: Earth Observation and Astronomy, 1994, Proc. SPIE, 2209, 36

Estrada, A. et al., 1998, Proc. SPIE, 3354

Farmer, C. B. 1987, High resolution infrared spectroscopy of the Sun and the Earth's atmosphere from space, Mikrochim. Acta (Wien), III, 189

Farmer, C. B. 1994, The ATMOS Solar Atlas, IR Solar Physics, 511

Farmer C. B., & Norton, R. H. 1989, Atlas of the infrared spectrum of the Sun and the Earth atmosphere from space. Volume I, The Sun, NASA Reference Publication 1224

Farmer C. B., and Norton, R. H. 1989, Atlas of the infrared spectrum of the Sun and the Earth atmosphere from space. Volume II, Stratosphere and Mesosphere, 650 to 3350 $cm^{-1}$, NASA Reference Publication 1224

Farmer, C. B., Raper, O. F., and O'Callaghan, F. G. 1985-1987, Final report on the first flight of the ATMOS instrument during the Spacelab 3 mission, JPL Publication 87, 32

Garnavich, P. M., Kirshner, R. P., Challis, P., Tonry, J., Gilliland, R. L., Smith, R. C., Clocchiatti, A., Diercks, A., Filippenko, A. V., Hamuy, M., et al. 1998a, ApJ, 493, L53

Garnavich, P. M., Jha, S., Challis, P., Clocchiatti, A., Diercks, A., Filippenko, A. V., Gilliland, R. L., Hogan, C. J., Kirshner, R. P., Leibundgut, B., et al. 1998b, ApJ, 509, 74

Graham, J.R., Abrams, M., Bennett, C., Carr, J., Cook, K., Dey, A., Najita, J., and Wishnow, E. 1998, PASP, 110, 1205

Graham, J. R. 2000, in Imaging the Universe in Three Dimensions: Astrophysics with Advanced Multi-Wavelength Imaging Devices. ASP Conference Series, W. van Breugel & J. Bland-Hawthorn (eds.), astro-ph/9907240

Griffin, M. J., Vigroux, L. G.; Swinyard, B. M. 1998, SPIRE: a bolometer instrument for FIRST, Proc. SPIE, 3357, 404

Gush, H. P., Halpern, M. & Wishnow, E. H. 1990, Phys. Rev. Lett., 65, 537

Haiman, Z. and Loeb, A. 1999, ApJ, 519, 479

Haiman, Z. & Loeb, A. 1998, ApJ, 503, 505

Hanel, R. A., et al. 1992, Exploration of the solar system by infrared remote sensing, Cambridge University Press, Cambridge, England

Hanel, R. A., and Conrath, B. 1969, Interferometer experiment on Nimbus 3: preliminary results, Science, 204, 972

Hanel, R. A., et al. 1970 The Nimbus 3 Michelson interferometer, Appl. Opt., 9, 1767

Hanel, R. A., Schlachman, B., Rodgers, D., and Vanous, D. 1971, The Nimbus 4 Michelson interferomter, Appl. Opt., 10, 1376

Hanel, R. A., et al., 1972, The Nimbus 4 infrared spectroscopy experiment, I. Calibrated thermal emission spectra, J. Geophys. Res., 77, 2639

Hanel, R. A., Schlachman, B., Breihan, E., Bywaters, R., Chapman, F., Rhodes, M., Rogers, D., and Vanous, D. 1972, The Mariner 9 Michelson interferometer, Appl. Opt., 11, 2625

Hanel, R. A., et al. 1972, Infrared spectrscopy experiment on the Mariner 9 mission: preliminary results, Science, 175, 305

Hanel, R. A., et al. 1980, Infrared spectrometer for Voyager, Appl. Opt., 19, 1391

Hanel, R. A., et al. 1979, Infrared observations of the Jovain system from Voyager I, Science, 204, 972

Hanel, R. A., et al. 1986, Infrared observations of the Uranian system, Science, 233, 70

Henderson, D. and Fasick, J.C., 1999 Inchworm Motor Developments for the Next Generation Space Telescope, SPIE 3429, 47

Hoffman, A.W. et al., 1998, Proc. SPIE, 3354, 24

Hogue, H. 1999, presentation to NGST detector workshop, 21 April 99, Balt. MD

Im, M. and Stockman, H.S. 1998, in Science with the NGST , eds., E.P. Smith and A. Koratkar, ASP Conf. Ser. vol 133, p. 263

de Zoeten, P., Haurer, R., and Birkl, R. 1993, Optical design of the Michelson Interferometer for Passive Atmospheric Sounding; Passive Infrared Remote Sensing of Clouds and the Atmosphere, Proc. SPIE, 1934, 284

Javelle, P., & Cayla, F. 1994, Infrared Atmospheric Sounding Interferometer (IASI) instrument overview; Space Optics 1994: Earth Observation and Astronomy, Proc. SPIE, 2209, 14

Kauffmann, G., Colberg, J.M., Diaferio, A., and White, S.D.M. 1999, MNRAS, 303, 188

Kawada, M., 1998, FIS: far-infrared surveyor on board the IRIS, Proc. SPIE, 3354, 905

Kirshner, R. P. 1999, Proc. Natl. Acad. Sci., 96, 4224

Kunde, V. G., et al., 1996, Cassini infrared Fourier spectroscopic investigation, Proc. SPIE, 2803, 162

Kozlowski, L. J., et al. 1998, Proc. SPIE, 3354, 66

Kneib, J.-P., Ellis, R.S., Smail, I., Couch, W.J., and Sharples, R.M. 1996, ApJ, 471, 643

Loeb, A. 1998, in Science with the NGST , eds., E.P. Smith and A. Koratkar, ASP Conf. Ser. vol 133, p. 73

Maillard, J. P. 1995, in 3D Optical Spectroscopic Methods in Astronomy, ASP Conference Series, Vol. 71, Eds. G. Comte, M. Marcelin, 316

Mather, J. C., et al. 1994, Measurement of the cosmic microwave background spectrum by the COBE FIRAS instrument, ApJ, 420, 439

Mather, J. C., Fixsen D. J., & Shafer, R. A. 1993, Design for the COBE Far Infrared Absolute Spectrophotometer (FIRAS), Proc SPIE, 2019, 168

Maymon, P. W., et al. 1993, Optical design of the Composite Infrared Spectrometer (CIRS) for the Cassini mission, Proc. SPIE, 1945, 100

McCreight, C. 1999, Development of Advanced Focal Plane Technologies for NGST, presentation to NGST detector workshop, 21 April 99, Balt. MD.

Menzel, E. 1999, NASA (GSFC), Private communication.

Mill, J. D. 1994, Midcourse Space Experiment (MSX), an overview of instruments and data collection plan: signal processing, sensor fusion, and target recognition III, Proc. SPIE, 2232, 200

Miller, J. L., 1994 Principles of Infrared Technology , Chapman & Hall, New York, 478

Pascarelle, S. M., Windhorst, R. A., Driver, S. P., Ostrander, E. J. & Keel, W. C. 1996, ApJ, 456, L21

Pascarelle, S.M. Windhorst, R.A., Keel, W.C., and Odewahn, S.C. 1996, Nature, 383, 45

Perlmutter, S., Aldering, G., Della Valle, M., Deustua, S., Ellis, R. S., Fabbro, S., Fruchter, A., Goldhaber, G., Groom, D. E. & Hook, I. M. 1998, Nature 391, 51

Perlmutter, S., Aldering, G., Goldhaber, G., Knop, R. A., Nugent, P., Castro, P. G., Deustua, S., Fabbro, S., Goobar, A., Groom, D. E., et al. 1999, Ap. J., in press, astro-phy9812133.

Persky, M. J. 1995, A review of spaceborne infrared Fourier transform spectrometers for remote sensing, Rev. Sci. Instrum., 66, 4763

Riess, A. G., Filippenko, A. V., Challis, P., Clocchiati, A., Diercks, A., Garnavich, P. M., Gilliland, R. L., Hogan, C. J., Jha, S., Kirshner, R. P., et al. 1998, ApJ, 116, 1009

Riess, A.G., Nugent, P., Filippenko, A.V., Kirshner, R.P., and Perlmutter, S. 1998, ApJ, 504, 935

Robichaud, J. L. et al. 1998, Proc. SPIE, 3354, 1068

Schmidt, B. P., Suntzeff, N. B., Phillips, M. M., Schommer, R. A., Clocchiatti, A., Kirshner, R. P., Garnavich, P. M., Challis, P., Leibundgut, B., Spyromilio, J., et al. 1998, ApJ, 507, 46

Schneider, P. and Kneib J-P. 1998, in The Next Generation Space Telescope: Science Drivers and Technological Challenges , 34th Liege Astrophysics Colloquium, p. 89

Schneider, P. and Seitz, C. 1995, AA, 294, 287

Seitz, C., Kneib, J.-P., Schneider, P., and Seitz, S. 1996, AA, 314, 707

Shimoda, H, & Ogawa, T. 1994, Interferometric Monitor for Greenhouse Gases; Infrared Spaceborne Remote Sensing II, Proc. SPIE, 2268, 92

Smail, I., Dressler, A., Kneib, J.-P., Ellis, R.S., Couch, W.J., Sharples, R.M., and Oemler, A. 1996, ApJ, 469, 508

Steinhardt, P. J. 1997 in Unsolved Problems in Astrophysics, J. N. Bachall & J. P. Ostriker, Eds. Princeton, NJ, p41

Stockman, P. ed., Next Generation Space Telescope: Visiting a time when galaxies were young, STSCI, 1997, 106

Thompson, R. et al., R. 1999, AJ, 117, 17

Vukobratovich, D., et al., 1998, Proc. SPIE, 3435, 9

Vural, K., presentation to NGST detector workshop, 21 April 98, Balt. MD

Wurtz, R. et al 1999, BAAS, 194, 91.01

Yan, L., et al. 1998, ApJ, 503, L19

Zachor, A, et al. 1994, Mid-course Space Experiment: Capabilities of the LWIR interferometer for remote sensing of trace constituents in the stratosphere and mesosphere; Atmospheric Propagation and Remote Sensing, Proc. SPIE, 2222, 99